Recent Developments and Future Challenges in Incremental Sheet Forming of Aluminium and Aluminium Alloy Sheets

Tomasz Trzepieciński [1,*], **Sherwan Mohammed Najm** [2,3], **Valentin Oleksik** [4], **Delia Vasilca** [4], **Imre Paniti** [2,5] **and Marcin Szpunar** [6]

1   Department of Manufacturing and Production Engineering, Faculty of Mechanical Engineering and Aeronautics, Rzeszow University of Technology, al. Powst. Warszawy 8, 35-959 Rzeszów, Poland
2   Department of Manufacturing Science and Engineering, Budapest University of Technology and Economics, Műegyetemrkp 3, H-1111 Budapest, Hungary; sherwan.mohammed@gpk.bme.hu (S.M.N.); imre.paniti@sztaki.hu (I.P.)
3   Kirkuk Technical Institute, Northern Technical University, Kirkuk 41001, Iraq
4   Faculty of Engineering, Lucian Blaga University of Sibiu, 550024 Sibiu, Romania; valentin.oleksik@ulbsibiu.ro (V.O.); delia.vasilca@ulbsibiu.ro (D.V.)
5   Centre of Excellence in Production Informatics and Control, Institute for Computer Science and Control (SZTAKI), Kende u. 13-17, H-1111 Budapest, Hungary
6   Doctoral School of Engineering and Technical Sciences, The Rzeszow University of Technology, al. Powst. Warszawy 12, 35-959 Rzeszów, Poland; d547@stud.prz.edu.pl
*   Correspondence: tomtrz@prz.edu.pl

Abstract: Due to a favourable strength-to-density ratio, aluminium and its alloys are increasingly used in the automotive, aviation and space industries for the fabrication of skins and other structural elements. This article explores the opportunities for and limitations of using Single- and Two Point Incremental Sheet Forming techniques to form sheets from aluminium and its alloys. Incremental Sheet Forming (ISF) methods are designed to increase the efficiency of processing in low- and medium-batch production because (i) it does not require the production of a matrix and (ii) the forming time is much higher than in conventional methods of sheet metal forming. The tool in the form of a rotating mandrel gradually sinks into the sheet, thus leading to an increase in the degree of deformation of the material. This article provides an overview of the published results of research on the influence of the parameters of the ISF process (feed rate, tool rotational speed, step size), tool path strategy, friction conditions and process temperature on the formability and surface quality of the workpieces. This study summarises the latest development trends in experimental research on, and computer simulation using, the finite element method of ISF processes conducted in cold forming conditions and at elevated temperature. Possible directions for further research are also identified.

Keywords: aluminium; aluminium alloys; forming strategy; incremental sheet forming; process parameters; sheet metal; SPIF; TPIF

1. Introduction

Aluminium is a metal of low density (2.6989 g/cm^3 at 20 °C), that is easy to form, with high electrical and thermal conductivity and high corrosion resistance. Annealed aluminium has the following properties: ultimate tensile stress, R_m = 70–120 MPa; yield stress, R_e = 20–40 MPa; and elongation, $A_{11.3}$ = 30–45%. Aluminium crystallises in a face-centred cubic (A1) lattice, which makes it a metal susceptible to cold and hot forming. The strength properties of aluminium and aluminium alloys can be increased by cold working, which, however, reduces its plastic properties [1]. In the strengthened state with a 60–80% degree of cold work, the strength of aluminium increases to 140–230 MPa. Aluminium has the ability to form a strongly adhering aluminium oxide layer on its surface, which is resistant to weather conditions and protects the metal against oxidation [2,3].

By adding alloying elements to aluminium, its strength properties can be increased even by several times [4,5]. The alloys obtained in this way are characterised by low weight and high impact strength. The greatest influence on increasing the hardness of aluminium is exerted by molybdenum, magnesium, cobalt, manganese, tungsten, vanadium, nickel, titanium, copper, iron, zinc and silicon [6,7]. Nickel and cobalt, as well as magnesium and manganese, increase the strength properties, and titanium and chromium affect grain refinement [8–10]. Copper lowers the casting shrinkage. The content of the main alloying elements in casting alloys reaches up to 30%, whilst in wrought alloys, such content is up to about 10%. Wrought alloys usually contain up to 5% of alloying elements and are used in the strengthened and heat-treated state. Casting aluminium alloys usually contain 5–25% of alloying elements. Under special conditions, casting aluminium alloys can be processed using metal forming methods [11,12]. Some alloys can be used in both the cast and wrought forms.

The ratio of the strength of aluminium alloys to their specific weight is greater than for steel. Moreover, their toughness does not decrease as the temperature is lowered; therefore, at low temperatures, they have a higher toughness than steel. However, Al-based alloys generally have a relatively low fatigue strength [13]. The fatigue life of aluminium alloys can be improved by adding transition metal elements such as Ti, V and Zr [14,15]. According to the EN 573-3:2019-12 [16] standard, aluminium alloys are classified according to their chemical composition in eight series 1xxxx–8xxx [16,17] (Table 1).

Table 1. Classification and main properties of the aluminium alloys.

Series of Al-Based Alloy	Main Alloying Elements	Properties
1xxx	lack (content of contaminations <1%)	good formability in cold forming and at elevated temperature, low strength, good resistance to corrosion, high electrical and heat conductivity
2xxx	Cu	low resistance to corrosion
3xxx	Mn	good formability but low strength, good weldability and corrosion resistance
4xxx	Si	high strength and corrosion resistance
5xxx	Mg	good corrosion resistance in salt water, good weldability and ability to anodising
6xxx	Mg + Si	high corrosion resistance, good formability
7xxx	Zn + Mg	the highest strength from all Al-based alloys, low and medium resistance to corrosion
8xxx	various alloying elements, the rest of aluminium alloys	-

The forming of materials by Sheet Metal Forming (SMF) is one of the most popular methods of obtaining finished products. Conventional methods of deep drawing sheet metal are carried out in cold, warm or hot forming conditions with the use of tools called stamping dies [18,19]. During SMF, the sheet is deformed by exceeding the yield stress of the material [20]. The disadvantage of conventional methods of sheet metal forming is the need to manufacture special tools adapted to the shape of the element; therefore, the use of conventional SMF methods with the use of stamping dies is suitable for medium- and large-scale production [21,22].

In Incremental Sheet Forming (ISF), as the alternative to the SMF method, the tool in the form of a rotating mandrel gradually sinks into the sheet, thus leading to an increase in the degree of deformation of the material [2,23]. This variation of ISF is called Single-Point Incremental Forming (SPIF). In Two-Point Incremental Forming (TPIF), a counter tool is used that moves on the opposite side of the sheet. The kinematics of these varieties will be introduced to the readers in Chapter 3. The use of ISF methods is economically justified in unit (i.e., medical implants) and small-lot production. One of the main limitations of ISF is the long machining time resulting from the point contact between the tool and the workpiece. The material is deformed locally along the given trajectory of the tool movement.

Both in conventional SMF and ISF methods, the increase in the strength of the drawpiece is related to the work hardening phenomenon of the sheet material [24–26]. An important advantage of ISF is the greater deformation limit of the material not causing sheet cracking than is the case with conventional SMF [27,28]. Similar to other sheet forming techniques, ISF also has some disadvantages related to the properties of deformable materials, which include geometric accuracy and springback [29].

In the last decade, an increase has been observed in works related to the incremental forming of the following lightweight alloy sheets: titanium and titanium alloys [30,31], aluminium alloys [32,33] and magnesium and its alloys [34]. These works are mainly related to the use of these alloys in the aviation [32] and space [35] industries, where, increasing, the share of lightweight metals in the entire structure is part of the efforts to reduce carbon dioxide emissions to the atmosphere. A brief overview of the state-of-the-art methods of incremental sheet forming for lightweight materials was provided by Trzepieciński et al. [36]. Over the last decade, aluminium has remained the most research-oriented material due to its wide application and applications in major industries due to its flexible properties [29]. On average, about 50% of the mass of materials used in the construction of passenger airplanes is provided by aluminium alloys [37]. The automotive industry is mainly interested in 5xxx and 6xxx series alloys. The 5xxx series alloys have excellent strength to weight ratios, formability properties and they are fully recyclable, the 6xxx series has the advantage of being versatile, heat treatable, highly formable and very weldable. Therefore, 6xxx alloys currently account for at least 80% of the volume currently supplied to automakers [38]. Aluminium alloys are used more and more commonly in the construction industry, where, while maintaining the same strength, it is possible to reduce the weight of the structure by about 50% in relation to steel materials [39]. The increasing demands on the use of lightweight alloys in a variety of applications have created a challenge in dealing with low formability materials at room temperature [36,40,41]. This has led to the development of heat-assisted ISF techniques that improve deformability in elevated temperature conditions [42,43]. These methods include induction heating-assisted ISF, laser-assisted ISF, electrically assisted ISF and combined electric- and stir-friction-assisted ISF [41,44,45].

Review papers found in the literature mainly concern a wide group of materials, but their concern is only the influence of selected forming parameters on selected properties of the drawpieces and ISF processing forces. Due to the difference in the mechanical properties of different materials, the conclusions for a given group of alloys may not be valid for other groups. In this paper, in the separate sections, the authors are focused on the effects of specific forming parameters on the formability and geometrical features of SPIFed and TPIFed aluminium and aluminium alloy drawpieces. This article provides an overview of the published research results on the influence of the parameters of the SPIF and TPIF processes on the formability and surface quality of the workpieces. Both cold forming and processes conducted at elevated temperatures were considered. The article summarises the latest development trends in experimental research, the analytical approaches used and the numerical simulations of ISF processes carried out. The advantages of applying thermally assisted methods of ISF to increase the formability of hard-to-deform aluminium alloys also forms one of the topics of this manuscript.

2. Methods of Review

The analysis of the literature in this article was carried out in accordance with Preferred Reporting Items for Systematic Reviews and Meta-Analyses (PRISMA) [46]. The review of scientific articles, review articles, chapters in monographs, conference materials and books indexed in the following major scientific bibliometric databases (IngentaConnect, Web of Science, ScienceDirect, Scopus, PubMed and EiCompendex) was limited to the English language. The patent databases of Espacenet, PatentScope and Google Patents were also explored. In fact, the scope of this review was limited to works written in the 21st century. However, significant earlier papers were also considered. Articles by the

same authors with similar content were not taken into account. In the same way, duplicate articles found in various databases and articles in conference proceedings, which were published in scientific journals in an extended version, were rejected from the review. We searched for articles where the main content was related to the incremental sheet forming of aluminium and its alloys. Next, the papers were divided according to the planned contents of individual subsections (methods of incremental forming, process formability of aluminium and aluminium alloys, accuracy in SPIF and TPIF, surface finish in ISF and thermal-assisted ISF).

3. Methods of Incremental Forming

3.1. Single- and Two-Point Incremental Forming

ISF is a sheet metal forming technique, where a series of small incremental localised plastic deformations are produced to form the final desired part [47,48]. ISF is one of the moderate, innovative sheet-forming technologies that does not use the traditional punch and dies. In ISF, a simple tool moves and follows a previously specified path with a defined strategy to incrementally deform a clamped sheet to produce a new part [49,50]. The ISF apparatus and process patent US3342051A for incremental dieless forming goes back to Leszak [51] in 1967; but the current conventional ISF is more similar to patent US3316745A [52], and it is identical to DE1527973A1 [53] submitted by Berghan and Murray. However, the relationship of the patents mentioned above to the emergence of ISF was rejected by Emeens et al. [54], who did not think that they represent the start of the current development of ISF. They state that the research published by Mason [55] is the origin of the beginning of the development of ISF. Later in 1984, Mason and his co-author Appleton published an article related to sheet metal forming for small batches using sacrificial tooling [56].

ISF technology can be divided into several types based on the number of contact points between the tool and the sheet. The two main varieties of ISF are as follows:

- Single Point ISF—only one contact point, in which one tool is used on one side of the sheet.
- Two Point ISF—two contact points from two tools, one on each side of the sheet.

The first patent mentioned above can be considered an SPIF, and TPIF was first presented by Matsubara [57]. Different subtypes of TPIF have been developed, utilising various support members; see the hierarchy graphic of the main methods of ISF in Figure 1.
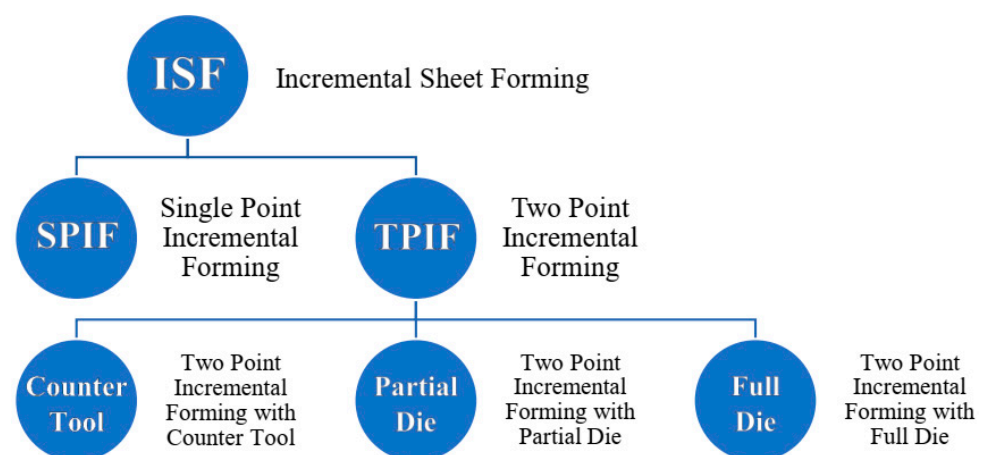

Figure 1. Main methods of incremental sheet forming.

In other categorisations, ISF can be classified into the following two main types: positive and negative; this definition is based on the concavity of the components, which can be concave up or concave down [58]. However, the one simple geometrical tool used in SPIF moves to form the sheet incrementally to finally form the desired part (Figure 2a), and this is identified as the most simplistic type of process within the ISF technologies [59].

In TPIF, also known as two-sided incremental sheet forming (TSIF), two contact points should encounter the sheet surface during the forming process, i.e., one contact point is the area between the forming tool and the sheet surface that is touched from the upper side and there is also a support contact on the opposite side of the sheet. An auxiliary tool, a counter tool, can be used as a support contact part in TPIS (Figure 2b); it can also be a partial die (Figure 2c) or a full die (Figure 2d). In TPIF with a counter tool, two independent tools are utilised to form the sheet, and a supplementary spindle is set on the opposite side of the main forming spindle of the forming machine. The gap between the two forming tools carried by the spindle holder, should be adjusted to the same sheet thickness. The gap should be readjusted during the forming process according to the thickness reduction following the sine law to ensure the forming tools are in contact with the sheet surface (Figure 2b). Related to the other two TPIF methods (Figure 2c,d), the sheet clamping rig must have an auxiliary movement to follow the step-down of the forming tool. The movement transfers the two clamping plates (blank holder and backing plate) as well as the sheet fixed between them, which slide down together guided on the assembly bars. The ability to move the TPIF rig noted above results in a significantly better geometric accuracy of the formed part, which enables one to control the sheet thickness distribution. Compared to SPIF (Figure 2a), TPIF produces more precise components in terms of geometric accuracy. Among the methods discussed, TPIF with a partial or full die is called positive incremental forming, and the other methods are called negative incremental forming [36].
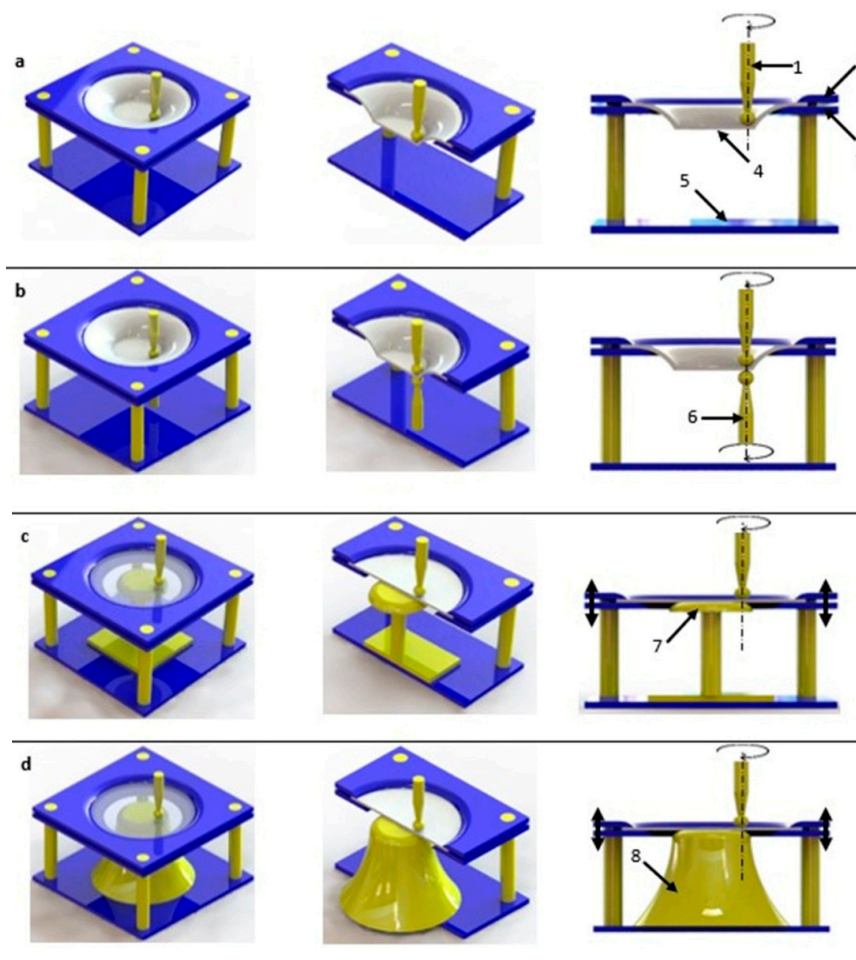

Figure 2. (**a**) SPIF, (**b**) counter tool TPIF, (**c**) partial die TPIF, (**d**) full die TPIF: 1—forming tool, 2—blank holder, 3—backing plate, 4—workpiece, 5—rig frame, 6—counter tool, 7—partial die, 8—full die.

Compared to SPIF, TPIF shows better formability and geometric accuracy [60]. Multi-stage TPIF is found to be effective in improving the thickness distribution of parts. Li et al. [61] analysed different tool path strategies in the multi-step TPIF of 5052 aluminium alloy sheets. The following four strategies were considered: the variable angle straight lines tool-path strategy, stretch-bend assist multi-stage strategy, parallel arcs tool-path strategy and parallel linear tool-path strategy. It was found that the thickness distribution of a specimen formed with the variable angle straight lines tool-path strategy is more uneven than in the other strategies.

3.2. Water Jet Incremental Forming

One of the problems of the SPIF and TPIF methods is the poor surface finish of the final components. Iseki [62,63] proposed a forming method that uses a high-pressure water jet (WJ). In this way, the friction occurring at the interface between the metallic tool and the workpiece is eliminated. The advantage of Water Jet Incremental Sheet Forming (WJISF) is that there is no tool wear and no contamination of the treated surface by grease. Moreover, as Jurisevic et al. [64] concluded, WJISF is preferable to conventional SPIF in environmental impact, except for one unfavourable aspect in terms of forming accuracy. The water pressure in WJISF is reduced to about one-tenth of that in water jet technology in order to prevent erosion of the workpiece. The plastic deformation of the workpiece material is induced with a certain force of water jet. In WJISF, the nozzle diameter is higher than in WJ, the flow of water volume is about ten times higher compared to the WJ cutting technique [64]. The relevant WJISF process parameters are shown in Figure 3. The surface pressure at the interface between the water jet and the workpiece p_S and the force of the water jet F_{WJ} are the most relevant WJISF parameters. The force F_{WJ} defines the maximum thickness of the blank that can be formed [64]. The water jet pressure plays an important role in the WJISF process. According to Lu et al. [65], if the forming pressure produced by the water jet is too high, it may cause high levels of deformation in a localised area, resulting in the wrinkling of formed parts.
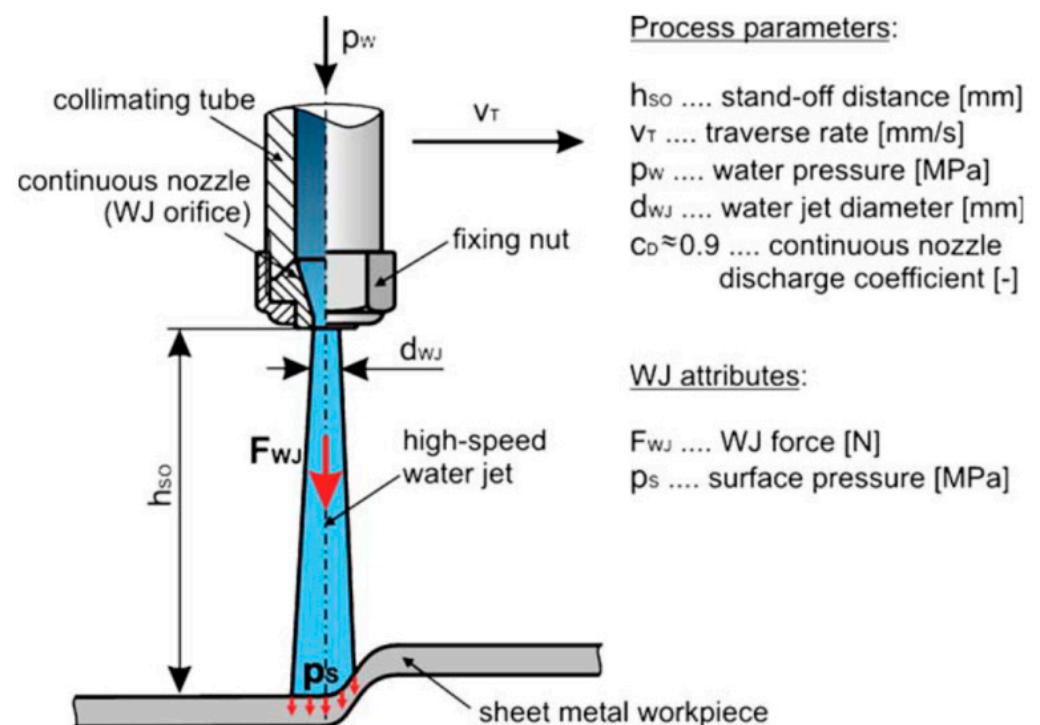

Figure 3. Process parameters of WJISF (reprinted with permission from [64]; Copyright © 2022, Springer-Verlag London Limited).

During the sheet deformation process, the water comes out from the nozzle in a closed circuit. Figure 4 presents a comparison between ISF and WJISF. Considering that WJISF is suited to unit and small-lot production, where the highest priority is to ensure a high-quality surface finish, increasing the processing time and energy consumption do not play a key role. The WJISF process is more flexible because, in principle, the process parameters can be changed online during the forming process. WJISF can be performed without lubrication, however. When the processing materials are susceptible to corrosion, special additives are required in the water [64].

Process attributes	ISF	WJISF
Flexibility	−	+
Surface integrity	−	+
Tooling requirements	−	+
Forming accuracy	+	−
Forming time	+	−
Energy consumption	+	−
Equipment costs	−	+
Environmental impact	−	+

Figure 4. Comparison between ISF and WJISF (reprinted with permission from [64]; Copyright © 2022, Springer-Verlag London Limited).

Zhang et al. [66] studied the high-pressure oil jet incremental forming of 0.3-millimetre-thick aluminium sheets by simulating the effect of the geometry of the conical nozzle on the dynamic pressure. They found that an oil pressure of 15 MPa was suitable for forming the aluminium sheet material. Emmens [67] used a set of rotating, columned water jets to expand and reshape beverage cans. He confirmed its high production efficiency for sheet metal parts with complex shapes when compared to the SPIF processes.

Jurisevic et al. [68] fabricated laminated tools with WJISF from aluminium sheets of different thicknesses. The laminated tools (Figure 5) were relatively easy to produce and did not significantly increase the total cost. Sajn et al. [69] carried out numerical simulations to obtain pressure and velocity distributions, taking into account turbulent fluid flow through the nozzle and the WJ. They found that the area on the metal sheet affected by the WJ pressure is significantly larger than the WJ cross section. The phenomenon of an enlarged pressure area was successfully verified by experiment. Teymoori et al. [70] used a coupled Eulerian–Lagrangian approach to simulate the WJISF forming process of a conical part using the three-dimensional Finite Element Method (FEM). The mechanics of liquid/solid interaction in WJISF were studied by Kai et al. [71] using a finite element-based numerical simulation. They modelled and simulated the water jet with a Computational Fluid Dynamics (CFD) approach. It was found that most of the thinning occurs in the former stage of WJISF and near the first path of the defined WJ trajectory.

According to the device covered by patent CN102218706A [72], a water jet head may be used for incremental sheet forming and cutting. The powerful impact force of the water jet is used to carry out WJISF on the plate. The fine features of the plate can be formed and cut by controlling the pressure of the water jet. In patent CN201110347675, He et al. [73] developed a water jet apparatus that rotates during machining and oscillates within a set range so that a high-pressure water column oscillates within the set range and rotates axially around the axis of the water column to complete the forming process.
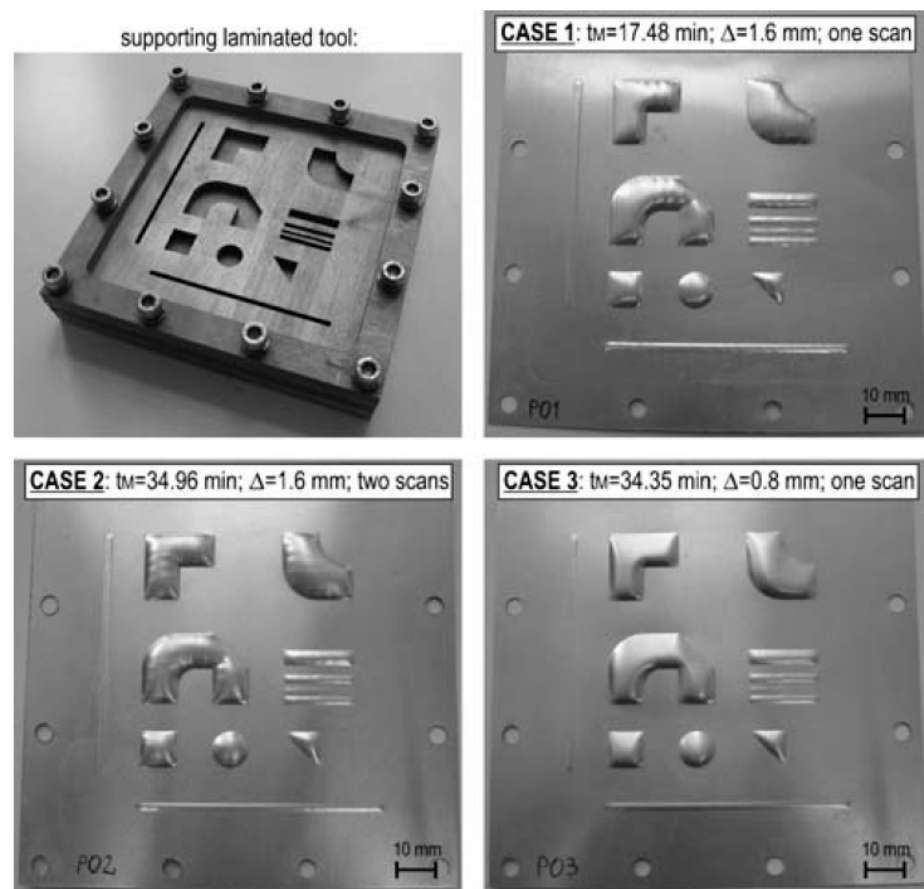
Figure 5. Laminated tools with various shapes and parts formed using different WJ trajectories (reprinted with permission from [68]; copyright © 2022, Springer-Verlag London Limited).

3.3. Electromagnetic Incremental Forming

Electromagnetic incremental forming (EMIF) uses a Lorentz's force occurring in a pulse magnetic field generated by circuits conducting a high-oscillation electric current [74]. The electric current produces a transient magnetic field around the coil that induces eddy currents in a metal workpiece. EMIF is a kind of powerful and high-speed forming technique where the deformation velocity can reach up to 300 m·s^{-1} [75] and the strain rate of the sheet metal is of the order of approximately 103·s^{-1} [76–78]. To precisely control the material behaviour in EMIF and obtain parts without defects, various techniques were employed, such as applying two-step forming [79], using tailored forming coils [80], selecting optimized process parameters [81], predicting formability and failure [82] and electromagnetic calibration [81,83]. EMIF is a powerful technique that can promote significant increases in the strain to failure in low ductility materials because of the strain rate and inertial effect [84].

The process of electromagnetic incremental forming technology is described by Feng et al. [84]. Firstly, the coil moved to the 0° position relative to the sheet, then the coil discharged (Figure 6a). After the coil discharge, the sheet incurs local deformation under the action of magnetic force. Then, the coil rotates along the sheet central axis, and the coil discharges again to a locally undeformed region (Figure 6b–e).
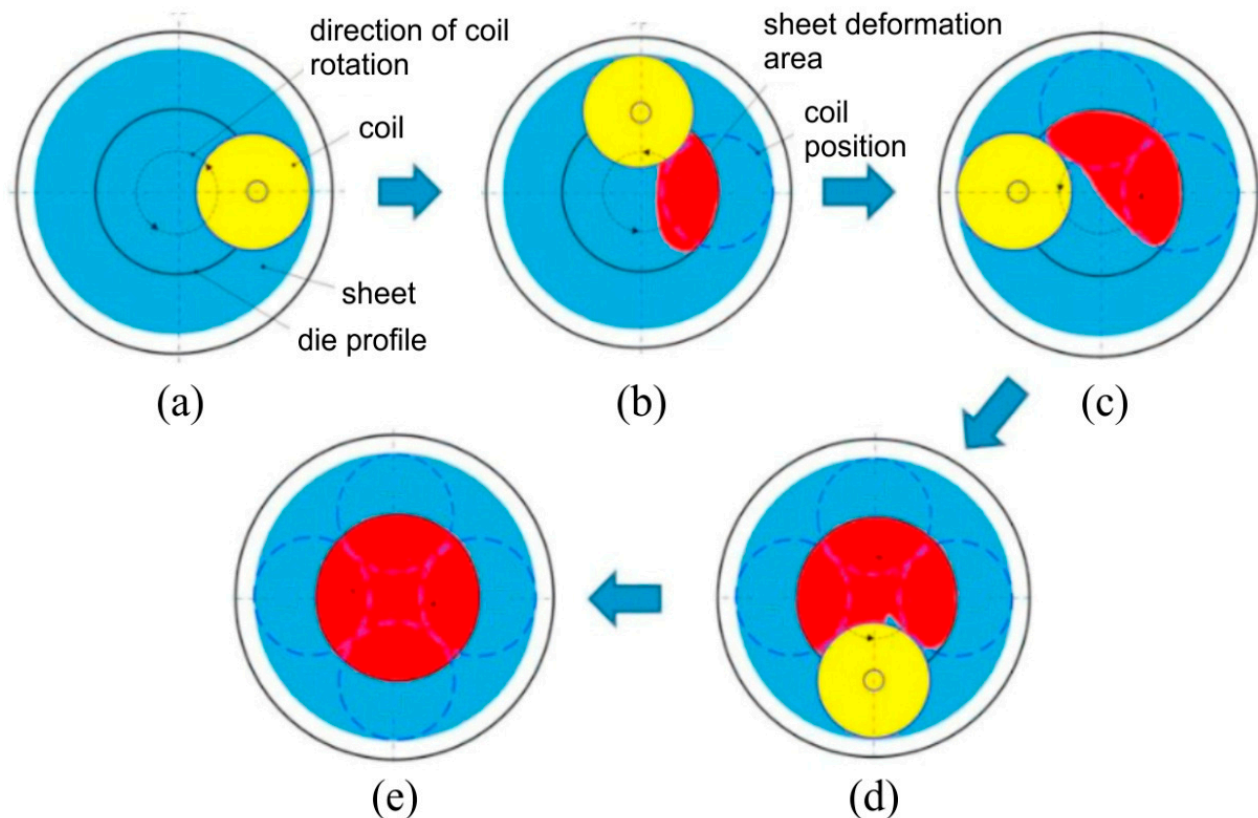
Figure 6. Electromagnetic incremental sheet forming technology: (**a**) the initial position of the coil and positions after rotation through (**b**) 90°, (**c**) 180°, (**d**) 270°, and (**e**) the region of plastic deformation of workpiece (reprinted with permission from [84]; copyright © 2022 The Author(s). Published by Elsevier Ltd.).

Although the electromagnetic incremental sheet forming is a relatively new technique, many scholars have investigated how to improve the formability of difficult-to-form materials and reduce springback. EMIF was firstly proposed by Cui et al. [85] to produce large-size parts made of AA3003 aluminium alloy sheets. The effects of the high-speed impaction interaction between a concave die and a 5052 aluminium alloy sheet, the coils moving trajectory and the discharge voltage on sheet formability were studied by Feng et al. [84]. It was found that the conventional EMIF method cannot form the bottom region flat part; it can only form the conical part. Imbert [86] demonstrated an increased formability when an AA5754 aluminium alloy sheet was formed into a conical die using EMIF. Long et al. [77] applied EMIF to manufacture a large-size AA2524-T3 aircraft skin with one-dimensional curvature. The feasibility of Ethe MIF method in forming specimen with a large size and one-dimensional curvature was verified. Liu et al. [87] investigated the effect of the shaping voltage on uniformity in EMIF based on dual coil with the interval moving strategy. They proposed a strategy for EMIF by multi-passes in each layer. During EMIF based on a dual coil with an interval moving strategy by two forming layers, better forming uniformity of AA5052 aluminium alloy sheets is found. Su et al. [88] investigated the deformation behaviours of a spherical crown-shaped thin-walled AA2219-O workpiece during a single layer forming of EMIF by means of finite element-based numerical modelling. It was found that the regions located outside the overlap region of coil positions deform insufficiently, leading to the poor overall uniformity of the component. The forming uniformity can be improved by properly reducing the first discharge voltage and increasing the last discharge voltage. Guo et al. [89] found that the two consecutive discharge methods of a small voltage followed by a high voltage in a fixed position was helpful for improving the forming depth and shape deviation to a die of the 2A12-T4 aluminium alloy panel.

EMF has many advantages that make it an attractive alternative to conventional SMF methods [90], such as the following:

- there is no mechanical contact with the work piece,
- no lubricants are needed,
- the process can be fully controlled,
- high technological flexibility,
- parts formed by EMF exhibit good surface quality and high dimensional accuracy,
- there is significant increase in workpiece ductility over conventional sheet metal forming methods,
- the formability limit is increased during electromagnetic forming due to high deformation velocity,
- the forming limit of the aluminium alloys can be improved by 10–14% [91] or even 2–3-fold [92], compared to the quasi-static loading conditions.

4. Process Formability of Aluminium and Aluminium Alloys

As is well known, aluminium and its alloys lend themselves to cold working operations. The plasticity of aluminium varies directly with the degree of purity. Thus, the higher the degree of purity is, the better the formability is. The plasticity of aluminium alloys is different, and it depends on the nature and quantity of the alloying elements. Of the alloying elements used in aluminium alloys, the magnesium content is of particular importance. An increased magnesium content decreases the plasticity of alloys. Other alloying elements that may be present in aluminium alloys are copper, iron, manganese and silicon. Their presence also leads to an increased mechanical strength and a decreased formability of aluminium alloys. The formability of aluminium and its alloys with respect to the main metal forming processes (bending, deep drawing, etc.) has been studied in numerous scientific papers. This sub-chapter aims to present the main studies related to the formability in incremental forming.

In order to assess the formability, a deformation mechanism and stress state analysis of the AA7075-O aluminium alloy in SPIF was performed by Neto et al. [93]. This analysis was based on both a numerical simulation using the finite element method and experimental investigations of the SPIF process for a frustum of the cone-type part with a wall angle of 45°. For the simulation, the hardening behaviour was implemented based on Swift's law and the Barlat criterion was chosen as the yield criterion. The major strain, minor strain (both on the outer and inner surface) and thickness reduction were determined. Following the analysis, it was found that the minor strain values are much lower than those of the major strain and that the major strain distribution is almost identical to the thickness reduction distribution. The authors of the paper also found that the deformation mode basically consists of a plane strain, as a result of the material predominantly deforming in the meridional direction. The stress analysis led to the conclusion that there is a negative mean stress in close proximity to the punch, leading to ductile fracture by nucleation.

Shrivastava and Tandon [94] assessed the formability and deformation mechanism of a face-centred cubic aluminium AA 1050 H14 alloy in SPIF based on the microstructure and texture analysis. The microstructure of the parts processed by SPIF was evaluated using the Electron Back Scatter Diffraction method and X-ray diffraction. The preliminary research presented in the paper was related to the SPIF processing of frustum of pyramid parts that were subsequently measured using Digital Image Correlation. By measuring the inner and outer surfaces of the cone, the thickness reduction was obtained for the processed parts. In parallel, the same geometry was obtained by numerical simulation using FEM, by means of the Altair software. In both experimental investigations and numerical simulations, data analysis was performed at four different stages (undeformed, early SPIF stage, intermediate SPIF stage and final SPIF stage). Subsequently, the average grain size was determined for these stages, showing a decrease in the average grain size from 42.40 to 11.05 μm on the frustum of the pyramid wall, in the area where the maximum values of the major strain were observed. The orientation of the individual grains was also studied, in order

to analyse the grain rotation angle. The conclusion drawn by the authors of the paper was that with the approach of the final stage, an increase in a large fraction of the high rotation angle and higher misorientation among the grains is observed. Since bending is the main stress in the first stages, an ultrafine grain structure is obtained. As the processing of the part progresses, the predominant stress is stretching, and therefore a fine structure is obtained, but with elongated grains. Another microstructural analysis was performed along the thickness direction. The appearance of slip bands is observed in the final stages of SPIF, which leads to the appearance and accumulation of dislocations. Another conclusion of the paper is that in the areas of the material where there is a biaxial mode of deformation, higher values of the thickness reduction are obtained, compared to the areas of the material in the plane strain condition.

The forming behaviour of an Al-Mg-Si alloy (AA-6061) was studied by Barnwall et al. [95] from both experimental and theoretical (numerical simulation) perspectives, showing a good correlation between the two approaches. The experimental investigations focused on the determination of the mechanical characteristics in three directions (rolling direction, transverse direction and diagonal direction), on the determination of the major strain, minor strain and thickness reduction using Digital Image Correlation, and then on the evaluation of the microstructural behaviour of the aluminium AA-6061 alloy based on electron backscattering diffraction. The geometry used in SPIF to evaluate the formability was a frustum of cone with a 45° wall angle and the punch trajectory was a spiral. The geometry of the analysed parts was divided into the following three zones, in order to assess the formability: a blank zone, a deformed zone situated on the wall of the part and an undeformed zone situated on the bottom of the part. The main zone of interest was, of course, the deformed zone, where the authors observed that the maximum values are obtained for both the major strain and the thickness reduction, which has an almost identical distribution to that of the major strain. It was also found that the direction of the major true strain is always perpendicular to the trajectory of the punch. The authors also presented the variation during the SPIF process of the major and minor strains for five radially arranged points, at equal distances, located in the deformed zone and named this graph the strain path curve. Regarding the microstructural changes of the AA-6061 alloy during the SPIF process, it was observed that while, initially, the material presented a higher volume fraction of cube and S textures, after the process, the deformed zone presented a considerable increase in the volume fraction of brass. An increase in the resistance to deformation in the diagonal direction with respect to the rolling direction and the transverse direction could also be observed, as a result of a higher Taylor in the diagonal direction.

A new test method for evaluating the formability in double side incremental forming has been proposed by Ai et al. [96]. Starting from an older test method, CBT (Continuous Bending under Tension), the authors of the paper proposed a method called TCBC (Tension under Cyclic Bending and Compression) for assessing the formability in DSIF. The method can be applied by making a device and mounting it on a uniaxial tensile test. The specimen is clamped between the uniaxial tensile test grips and stressed in the longitudinal direction. A cylinder presses on the surface of the specimen producing bending. The cylinder also moves cyclically along the specimen. A second cylinder presses and moves at the same time as the first cylinder on the opposite side of the specimen, producing compression. The scheme of the proposed test method is shown in Figure 7.
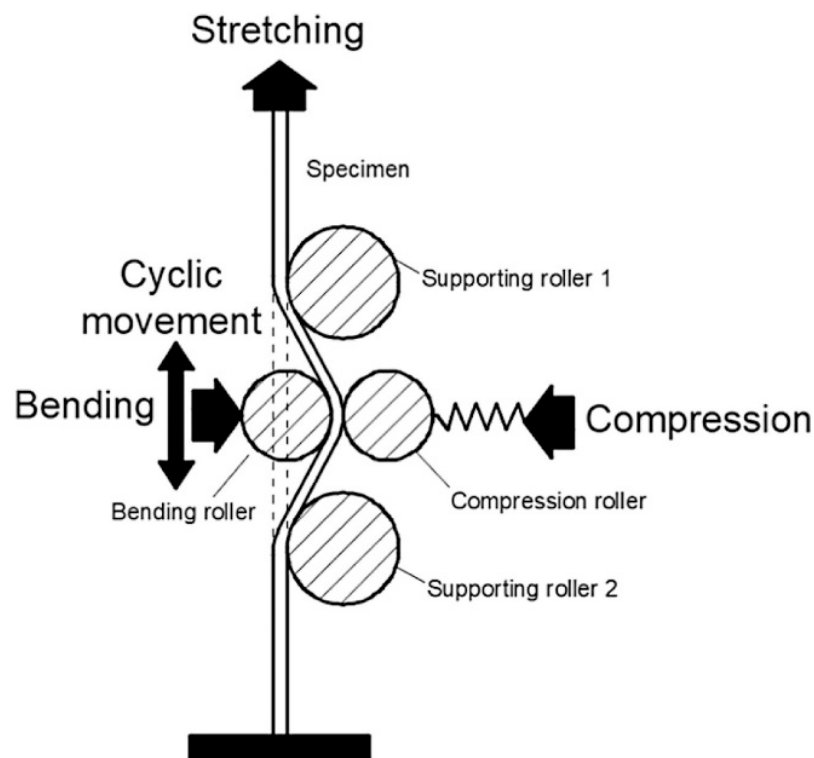
Figure 7. Schematic of the Tension under Cyclic Bending and Compression test concept (reprinted with permission from [96]; copyright © 2022 Elsevier B.V. All rights reserved.).

The stress state induced by this method is much more similar to that present in DSIF, where the compression also has an important effect. Two aluminium alloys were tested in the study, AA5251-H22 and AA6082-T6, respectively. Tests were performed for simple tension, tension and cyclic compression, tension and cyclic bending and tension and cyclic bending and compression. An increase in elongation of almost seven times was found for specimens stressed in tension and cyclic bending and compression, compared to those stressed in simple tension. The major strain–minor strain diagrams were also plotted. The DSIF process was then simulated using the finite element method and the major strain–minor strain diagrams were plotted in this case also. It was found that the proposed method can be used successfully for a more accurate evaluation of the formability in DSIF.

The issue of reusing parts obtained by metal forming technologies (in most cases by deep drawing) was studied by Ingarao et al. [97]. In order to reduce metal waste, scrap parts can be reused if they are processed by SPIF. The authors of the paper analysed the behaviour of parts initially processed by deep drawing and then subjected to the SPIF process. An AA-5754 H22 aluminium alloy with 0.5 mm thickness was chosen for the study. The following two cases were analysed: one in which the SPIF geometry is located at a distance from the deep-drawn area, and another in which the SPIF geometry is close to the deep-drawn area. For the first case, a frustum of cone geometry (with small diameter) was obtained on a square-box-type part formed by deep-drawing, while for the second case, a frustum of pyramid geometry was obtained on a square-shape-type part formed by deep-drawing. In the second case, the dimensions of the two geometric shapes are similar. For this situation, the following two wall angles were chosen to be processed by SPIF: 45° and 60°. In the first case, the thinning of the material produced by the SPIF process did not affect the geometry already achieved by deep drawing, due to the fact that the two geometries practically do not interfere. In the second case, even if a significant increase in strain and thickness reduction was observed in the areas where the two geometries are close together, no fractures occurred in the material.

The studies carried out to assess the formability in SPIF of aluminium and aluminium alloys did not only concern flat sheets with uniform thickness. Do et al. [98] published

a paper that addresses the formability of 3D structured aluminium. In their paper, they compared the forming behaviour of an Al3004-P aluminium alloy presented in the following two forms: a flat aluminium sheet and an embossed aluminium sheet. The embossed model was achieved by means of two embossed rollers of conical shape, obtaining a model with a pitch of 6.4 mm and a height of 0.7 mm. The first step consisted of research carried out to determine the mechanical characteristics by means of the uniaxial tensile test. For the embossed aluminium sheet, specimens were taken in the following two directions: parallel to the embossed pattern and at 45° to the direction of the embossed pattern. For the embossed specimens taken in the parallel direction, an increase in elongation was observed compared to the flat specimens, as well as an increase in the hardening exponent. For the specimens taken at 45°, the results were similar to those of the flat specimens. Using a CNC milling machine, parts were made by SPIF for a frustum of pyramid geometry. An increase in the maximum wall angle to 62° was found in the case of the embossed specimens, compared to 60° in the case of flat specimens when using an inward path, and a maximum wall angle of 64° was found in embossed specimens when using an outward path. The authors of the paper then plotted the FLC in SPIF for the embossed aluminium Al3004-P material, based on the major and minor strain.

Abd et al. [99] presented the possibility of using the SPIF process in the forming of an Al/SUS bimetal sheet. To evaluate the formability of bimetallic sheets, they used an Al1050 sheet with 1.5 mm thickness and SUS304 with 0.5 mm thickness. After the hot rolling process, a thickness of 1 mm of the composite sheet was obtained, achieving a thickness reduction of 50%. The parts were formed in two variants, with the aluminium coming into contact with the punch (AL/SUS) and with the steel coming into contact with the punch (SUS/AL). The geometry of the parts made was a frustum of a pyramid with a variable angle, in order to determine the maximum wall angle at SPIF. The process parameters were varied, namely, the punch diameter (from 10 to 20 mm) and the vertical step (from 0.15 to 1 mm). It was found that regardless of the process parameters used, the maximum value of the wall angle is obtained in the case where the punch comes into contact with the steel (SUS/AL). Using Digital Image Correlation (DIC), the major strain and minor strain, as well as the FLD, were determined for these bimetallic materials. As expected, the position of the FLD line in SPIF in the SUS/AL case is higher than in the AL/SUS case. In addition, the negative slope of the line in the AL/SUS case is observed to be greater in absolute value than in the SUS/AL case. All these conclusions lead to the idea that, in terms of formability, it is preferable that the punch is in contact with the steel in the case of these bimetallic materials. The authors also evaluated the influence of the punch diameter and vertical step on the maximum wall angle in bimetallic materials and concluded that at a small value of the vertical step (0.15 mm), increasing the punch diameter leads to a decrease in the maximum wall angle, while at a large value of the vertical step (1 mm), the effect is reversed, i.e., increasing the punch diameter leads to an increase in the maximum wall angle.

4.1. Forming Limit Diagram

One of the first studies related to the aluminium formability (for 3003-0 and 5754-0 aluminium sheets) is that of Jeswiet et al. [100]. The study began by obtaining a linear dependence relation between the wall angle and the initial thickness of the material for the two mentioned aluminium alloys. The authors of this study were among the first to draw the FLD for the incremental forming of aluminium alloys. To obtain the FLD, experimental investigations were carried out up to the breakage of the material for several types of geometries: the frustum of a cone shape, hyperbolic shape, hemispherical (dome) shape, the frustum of a pyramid shape and a complex shape with five lobes. It was thus found that for the frustum of cone-shaped parts, the FLD is represented as a line with a negative slope (of value −1) located in the first quadrant of the major and minor strain (that of the positive biaxial strains). For the other types of geometries, the slope of the line located in the same quadrant is also negative, but of a much larger value (between −30 and −40).

The authors proposed constructing the FLD based on the two lines, thus covering most types of part geometries obtained by SPIF.

Another paper, published by Mugendiran and Gnanavelbabu [101], performed a comparison of the FLDs and thickness reduction distribution for two parts, a frustum of the pyramid-type part and a frustum of the cone-type part. The material used in the paper was aluminium AA5052. For both parts of the geometries, FLDs were plotted as lines with a negative slope, located in the quadrant with positive major and minor strains. The authors observed that higher values of the major and minor strains are obtained in the case of the frustum of cone-type parts and, consequently, the FLD line for these parts is found above the FLD line of the frustum of pyramid-type parts. Another conclusion is that the slope of the FLD line for the frustum of cone-type parts is greater than that of the frustum of pyramid-type parts. Comparing these results with the ones obtained when measuring the thickness reduction for the two types of geometries, it is found that the frustum of cone-type parts has a lower thickness reduction than the frustum of pyramid-type parts. Both conclusions lead to the idea that the formability of parts with no corners, made of smooth trajectories and without sudden changes of trajectory, is better.

Madeira et al. [102] proposed another study to assess the formability and determine the FLD for SPIF. Aluminium AA1050-H111 with a thickness of 1 mm was used for this research. The authors used circle grid analysis to measure the major strain and minor strain, and the tests were continued until the circumferential fracture occurred. The aim of the research was to improve the understanding of the behaviour of aluminium in SPIF by combining several tests: the double notched uniaxial tensile test, conventional formability tests (Nakajima test, circular and elliptical bulge test and hemispherical dome test) and a test on a frustum of a cone-type part made by SPIF. The FLCs (forming limit curves) were plotted on the basis of the conventional tests, while the FFLs (forming fracture lines) were plotted on the basis of the double notched uniaxial tensile test. In order to obtain the frustum of cone-type parts by SPIF, different diameter punches (4, 6, 10, 15 and 25 mm) were used. By comparing the results obtained in SPIF with those of the FLC and FFL, the authors proved that the fracture in SPIF occurs by tension and the fracture based on shear stresses (in-plane or out-of-plane) cannot be questioned in SPIF.

Kumar and Maji [103] analysed the formability of aluminium alloys in SPIF, determining the FLC based on the groove test and the deformation instability method. The material used for the formability analysis was an AA5083 aluminium alloy, an alloy with good thermal conductivity and corrosion resistance, accompanied by good strength. The mechanical properties of the aluminium alloy were determined by conducting uniaxial tensile tests on the rolling direction, transverse direction and at 45° to the rolling direction. The FLCs for SPIF were then plotted and compared with the FLCs obtained in conventional forming using the Marciniak–Kuczynski test. The authors concluded that the formability in SPIF is improved by 60–80% compared to the conventional forming processes. Parts with different wall angles were then made. The analysis continued with the plotting of the FLCs in SPIF for different vertical steps, different speed rates and different rotation speeds. It was concluded that increasing the vertical step leads to a decreased formability, while increasing the feed rate and rotation speed leads to an increased formability of the AA5083 aluminium alloy. The FLC was also plotted for heat-assisted incremental forming, where the heating took place up to 300 °C. It was, thus, observed that increasing the temperature significantly influences the maximum wall angle, which can be increased by up to 3° in heat-assisted incremental forming.

Several studies have recently focused on the application of SPIF to tailored welded blanks. A recent paper conducted a comparative study on the FLD for welded blanks made of AA6061 aluminium with a thickness of 2 mm and dimensions of 250 mm × 250 mm [104]. In fact, this study compared the FLD lines for different positions of the welding line relative to the rolling direction. After selecting the optimal direction, the Response Surface Methodology (RSM) was used to identify which parameters are optimal in terms of the friction stir welding process. The specimens were welded so that the welding line was

parallel to the rolling direction of both sheets, perpendicular to the rolling direction of both sheets and forms an angle of 45° with the rolling direction of both sheets. The frustum of cone was chosen as the geometry used to determine the FLD. The results obtained led to the conclusion that the best results in terms of formability are obtained when the welding line is positioned at an angle of 45° with the rolling direction of both sheets. The authors correlated these results with the strain hardening exponent values obtained for the same types of specimens, obtaining the highest value in the case of those at an angle of 45° with the rolling direction of both sheets.

Another piece of research, also related to the evaluation of the formability of friction stir welded blanks of aluminium alloys during SPIF, was published by Carlone et al. [105]. The aim of this study was to determine the optimal friction stir welding parameters so that the specimens produce the best results in terms of formability. The aluminium alloy used for this research was 6082-T6. Unlike other studies on the formability of friction stir welded blanks of aluminium alloys, which focused either on producing the frustum of cone- or the frustum of pyramid-shaped parts with a constant wall angle, or on evaluating the formability based on groove tests on different directions, this research focused on producing the frustum of cone-shaped parts with variable wall angles. Thus, the authors were able to evaluate, based on the maximum frustum of the cone height, the maximum wall angle at which the fracture occurs in SPIF. Five types of specimens with different rotational speeds and feed rates were made by friction stir welding, and their results were compared with a specimen made of base material and a specimen obtained using the tungsten inert gas (TIG) welding process. A strong decrease in formability was observed in the specimen obtained using TIG. It was also noted that the best results (maximum frustum of cone height and maximum frustum of cone wall angle), even better than those of the base material specimen, were obtained for the specimen with a rotational speed of 1200 rpm and a feed rate of 70 mm/min. FLDs were also plotted for these specimens and compared with those obtained in the conventional metal forming processes.

4.2. Effect of Process Parameters on Formability

One of the most important parameters considered for improving the formability in SPIF is the forming strategy. Buffa et al. [106] used the finite element method (FEM) and the Circular Grid Analysis (CGA) to highlight which multi-step forming strategy leads to better results in terms of increasing the formability for AA1050 sheets with 1 mm thickness. The investigations were performed both numerically, using the finite element method, and experimentally, for square-cup-shaped parts with a 90° wall angle. The forming process was continued until the breakage of the part. The following three types of strategies were considered: a strategy by which a progressive increase in the wall angle is achieved (strategy A), another strategy by which the part side is increased and thereby leads to an increase in the wall angle (strategy B) and a last strategy using a non-horizontal path plane (strategy C). While strategies A and B are mono-directional strategies, strategy C is a multi-directional strategy, whereby the part goes through different stages until the final shape is reached. All these strategies are presented in Figure 8. In the parts processed using the first two strategies, the fracture occurred in the corner area of the part when the angle exceeded 70°. In the parts processed using strategy C (a non-horizontal path plane), no material breakage occurred. Using CGA, the authors also plotted the minor strain–major strain diagrams for the processed parts. For strategy C, these diagrams were also presented for the intermediate stages of the part up until the final shape. Their analysis found that there is a substantial increase in formability when using this type of strategy, mainly due to the redistribution of material over the thickness of the part.
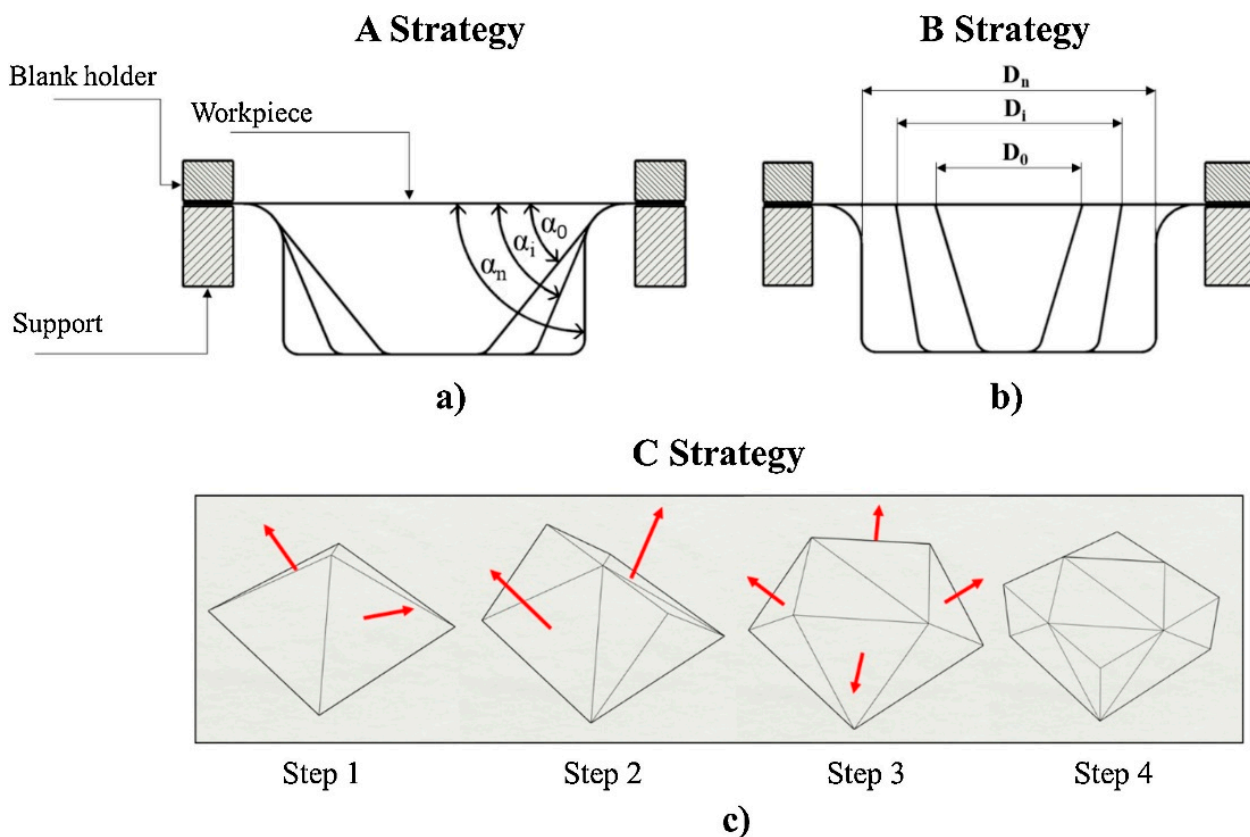
A Strategy

a)

B Strategy

b)

C Strategy

Step 1   Step 2   Step 3   Step 4

c)

Figure 8. The three strategies used (**a**) A strategy, (**b**) B strategy and (**c**) C strategy (reprinted with permission from [106]; copyright © 2022 The Society of Manufacturing Engineers. Published by Elsevier Ltd. All rights reserved).

The effect of the punch geometry, punch diameter, side radius of the flat end of the punch and a radius of an active surface of the punch on the formability of AA2024-O aluminium alloy sheets in SPIF was studied by Kumar et al. [107]. They chose the forming depth of the frustum of cone-shaped parts as a formability indicator. Two punch geometry shapes were chosen, a hemispherical one and a flat end one, as well as three values for the punch diameter, three values for the radius of the active surface of the punch and two values for the side radius of the flat end for each punch's geometry. Parts with three values of the wall angle, 60°, 65° and 70°, were also made and three values of the vertical step, 0.2, 0.5 and 0.8 mm, were used. The punch trajectory was a helical one. The processed parts were scanned using a dual CCD camera. It was observed that decreasing the punch diameter and radius lead to decreased formability and that the punch with a hemispherical shape leads to increased formability. It was also found that decreasing the wall angle and vertical step leads, as expected, to increased formability.

Baruah et al. [108] conducted a study that aimed to optimize the process parameters for the SPIF forming of an AA5052-H32 aluminium alloy with 1 mm thickness. The objective of the optimization process was to simultaneously increase the formability and improve the surface quality by reducing the roughness, and the following parameters were considered: vertical step, feed rate, rotational speed and lubrication. These were varied on three levels each, as follows: 0.2, 0.5 and 0.9 mm for the vertical step; 200, 500 and 800 mm/min for the feed rate; and 150, 400 and 800 rpm for the rotational speed and dry, grease and oil for lubrication, respectively. The Grey relational analysis (GRA) was used as the optimization method, while the test to evaluate the formability was the groove test, performed in the rolling direction, transverse direction and diagonal direction (45° to the rolling direction). The maximum depth of the parts before the fracture occurred, as well as the roughness of the surface coming into contact with the punch, were measured. Based on Taguchi's

orthogonal array, Grey relational analyses and ANOVA, the following optimal values were obtained, which allow both the increase in the formability of the AA5052-H32 aluminium alloy during SPIF and the reduction in the roughness: vertical step: 0.5 mm, feed rate: 200 mm/min, rotation speed: 150 rpm and using a grease as lubrication.

Another paper that studies the formability of an aluminium friction stir welded blank, this time during single point incremental forming versus two-point incremental forming, is a study conducted by Ebrahimzadeh et al. [109]. The material used in the paper is aluminium 5083. The first research of the authors concerns the identification of the influence of the friction stir welding process parameters (rotary speed, travel speed and plunge depth) on the mechanical characteristics of the aluminium welded blanks determined on the basis of the uniaxial tensile test. The parts were then processed by SPIF and TPIF with two values of the wall angle, 63° and 73°, until the breakage occurred. It was found that for both values of the wall angle, the maximum height obtained was greater in the case of TPIF, the greatest difference occurring for the wall angle of 63°. Based on the Response Surface Methodology (RSM), an algorithm was developed to choose the optimum values of the incremental forming process factors. The influencing factors considered for both variants of incremental forming were the vertical step, rotational speed and feed rate, each of which had three levels of variation. Thus, the following values were chosen: 0.2, 0.4 and 0.6 mm for the vertical step; 0, 400 and 800 rpm for the rotational speed; and 200, 400 and 600 mm/min for the feed rate. The thickness reduction was measured to evaluate the formability, while the springback was measured to evaluate the geometrical precision for all the possible cases resulting from the combination of the previously mentioned parameters. It was, thus, concluded that increasing the rotational speed leads to an increase in the thickness reduction and consequently to a reduction in formability, that increasing the feed rate leads to a decrease in thickness reduction and consequently to an increase in formability and that the vertical step has very little influence on the thickness reduction and formability.

Vanhove et al. [110] presented a study on the formability of aluminium alloys processed by SPIF at a cryogenic temperature. They performed tests on two aluminium alloys, AA5083-H111 and AA1050-H24, at the following three different temperatures: 293, 193 and 78 K. Preliminary investigations (uniaxial tensile tests) carried out at the same temperatures led to an increase in the formability of the two alloys as the forming temperature decreased. In order to obtain the parts by SPIF, a cryogenic cooling clamping system was built. The geometry of the parts made was a frustum of a cone. The parts were obtained by dipping in LN_2, both without lubrication and with graphite coating. The SPIF process at low temperatures was not possible without graphite coating, the parts showing fractures regardless of the wall angle. The parts with graphite coating also showed a decrease in formability with a decreasing temperature, obtaining a maximum wall angle of 74° at 293 K, 72° at 193 K and 64° at 193 K. The authors indicated the change in the formability behaviour with respect to the uniaxial tensile test, the main cause of this behaviour being the increased level of stress triaxiality in the parts formed at the cryogenic temperature.

The influence of ultrasonic vibration on the formability of 1060 Aluminium material was evaluated by Yang et al. [111]. The study was conducted using the Abaqus finite element software on a frustum of cone geometry. The punch, in addition to the movement on the trajectory required for the part forming, was also imprinted with a sinusoidal (vibratory) movement with different amplitudes and different frequencies. Following the analysis, the plastic strain along the x, y and z axes and the thickness reduction were determined in order to estimate the moment when the breakage of the material occurs. The authors started by studying the influence of ultrasonic vibrations on the maximum wall angle in the parts processed by SPIF. The frequency was maintained at a constant value of 24 KHz and the amplitudes were of 0, 2, 4, 6, 8 and 10 μm. The highest wall angle value was obtained for a frequency of 6 μm. The respective frequency value (of 6 μm) was then maintained at a constant, and the amplitude was varied from 10 to 25 KHz. It was thus concluded that the highest formability is obtained at an amplitude of 25 KHz

and a frequency of 6 μm, for a 1060 aluminium sheet. The results obtained by numerical simulation were then validated experimentally, and a punch clamping system, equipped with an ultrasonic generator with a maximum power of 2 kW, was built.

5. Accuracy in SPIF and TPIF

ISF is a more suitable solution than the conventional sheet forming processes as far as prototype manufacturing or small batch production processes are concerned. Many process parameters affect the formed part's quality and accuracy; however, improperly selecting these parameters can cause a crack or fracture to appear during the process before achieving the desired shapes. ISF still has disadvantages in terms of the geometric accuracy of the components, in particular due to springback, path compensation and pillow effects. To form sheet material incrementally with more accuracy, patent US7984635B2 [112] by Callebaut and co-inventors from the University of Leuven, Belgium, dating from 2011, locally applied dynamic heat to the contact zone by moving a laser that moves synchronically in TPIF using a partial die. In patent US10010920B2 [113] and similar patents CN102343386B [114], DE102011079734A1 [115] and RU2576792C2 [116], Ren and co-workers [113] incrementally formed a part using TPIF in which two forming tools move along multiple axes under the control of an electronic controller that decreases the gap between the tool and the sheet, thus improving geometric accuracy. In another patent, US8322176B2 [117], by Johnson and his co-workers and an identical Chinese patent, CN201744547U [118], the first forming tool moves in various directions along the upper sheet surface to form a sheet and improve the surface quality and geometric accuracy. A second tool moves in multiple directions along the lower sheet surface. The first and second forming tools pass using first and second manipulators configured to move the forming tools according to the predetermined path strategies. In patent EP2505279A1 [119], a device for two-sided incremental sheet forming was invented to reduce the influence of the acting force on the lower forming tool and to stabilise and guide both forming tools to ensure accurately formed components. To prevent ridges and ploughing in the formed sheet because of the incremental step, patent US11072015B2 [120] by Roth et al., which is the same as patent US62311689 [121], proposed a tool and method to incrementally form a sheet by single point, double-sided and multi-axis approaches. This patent proposes the generation of a high frequency between the two steps, basically vibrating the forming tool in all directions, up and down, side to side, inside and outside, or any combination of these, to provide a better surface, increased formability and greater geometrical accuracy.

The accumulative double-sided incremental forming (ADSIF) system in patent US9168580B2 [122] and an identical patent in WIPO WO2013062827A1 [123] was invented by Cao and Malhotra. Patent US20210237140A1 [124] proposed double-sided incremental tools for enhanced accuracy. The tool includes a sleeve with a hollow interior space to position the contact element inside the hollow interior space of the sleeve. The aforementioned patent is identical to EP3858511A1 [125] and CN113198919A [126]. The geometric accuracy achieved with ADSIF is noteworthy when compared to SPIF and DSIF. Continuous tool lines on both sides of the formed part indicate no contact loss between the forming tools and the sheet surface. The innovative tools proposed in patent US8021501B2 [127] by Kiridena et al. were used to assure dimensional accuracy and accessibility in the incrementally formed part. They indicated that forming tool deflections significantly affects the geometric accuracy as the shank length becomes longer and the diameter becomes smaller, and the flat underside of the doughnut-shaped tips improved the geometric accuracy of the part. However, it stated that elastic deformation at the tool tip will produce dimensional inaccuracies of the formed part, and the plastic deformations will permanently damage the forming tool if a flat tool with the smallest corner radius is used because of a reduction in springback.

5.1. Springback Reduction

Inaccuracy in a component's geometry discourages the use of ISF as an essential industrial process and the use of this technology by manufacturing companies in place of conventional methods. One of the main criteria that affect the accuracy of the components is springback. Two scenarios cause springback; the first is local springback because the sheet placed behind the advancing forming tool has a tendency to return to its initial position. The second is global springback in which springback occurs after the release of the clamping on the sheet as the remaining residual stresses in the unconstrained material of the part formed using ISF are released [128]. Besides the above-mentioned two scenarios of springback, Gatea et al. [129] mentioned another type that occurs with the displacement of the tool called a continuous local springback. Furthermore, they stated that researchers gave particular consideration to the ISF process parameters on springback and accuracy because it is one of the main significant drawbacks of the process. Therefore, Bambach et al. [130] stated that multistage incremental forming reduces local elastic deformation and local springback (Figure 9) at the end stage of forming, which, in general, increases the accuracy of the final product. Springback can be affected by the following various factors: tool shape and size, rotation speed, feed rate, initial sheet thickness, wall angle and residual stresses. To reduce springback, many researchers have provided different solutions.
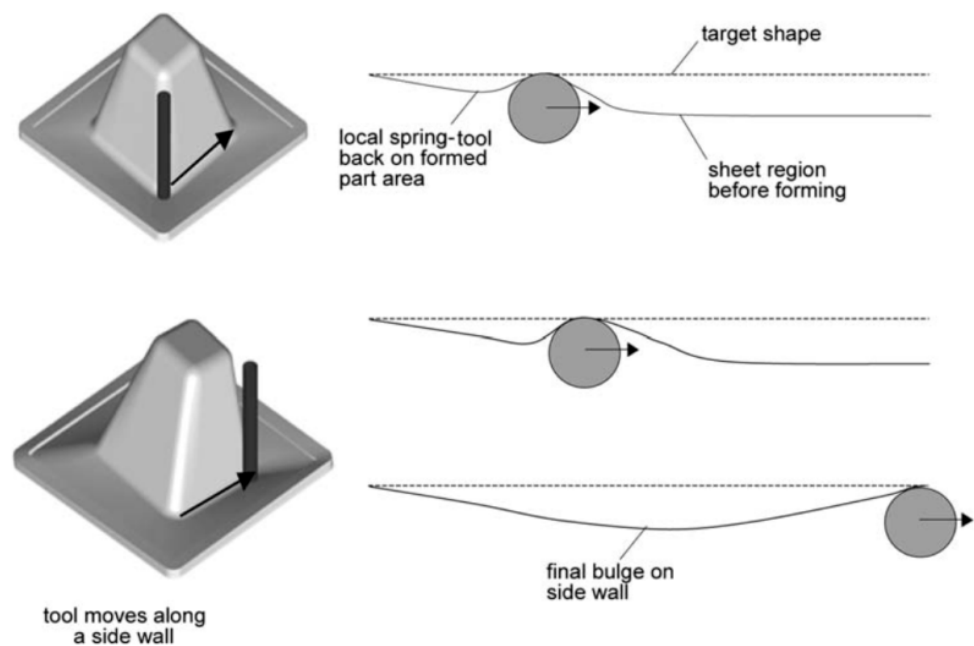

Figure 9. Scheme of local springback in SPIF (reprinted with permission from [130]; copyright © 2022, German Academic Society for Production Engineering (WGP)).

A method is proposed for mechanically deforming sheet material to decrease springback in patent EP0055435A2 [131], published in 1982, and US4373371A [132], published in 1983 by Liu. The electrically assisted double-sided incremental forming invented in patent US8741079B2 [133], as with WIPO WO2012030835A2 [134], by Roth and Cao, can double-side form a sheet incrementally and directly apply electricity to the formed part. The current can be switched on before/after starting the forming process and/or switched off before/after the ending of the forming process. The invention can reduce the forming force, increase formability and reduce any springback. The first patent, US8021501B2 [135], was submitted by Roth and granted in 2011. It proposes the application of a direct electric current through the SPIF apparatus to reduce any springback. Patent US10500629B2 [136], dating from 2019, was also submitted by Roth and, together with the identical WIPO patent WO2016/057688Al [137], provides a method for reducing springback using electrically assisted manufacturing (EAM) on a 2024-T3 aluminium sheet that is 0.5 mm thick.

The influence of using direct current on the reduction in springback on 6061 aluminium sheets formed by SPIF has been described by patent US9951397B2 [138]. This asserts that reduced springback can be obtained by increasing the current density applied until the springback is eliminated at a current density of 120 A/mm^2. Patent US6971256B2 [139] by Okada et al. provides a method and apparatus for TPIF to reduce springback caused by supplying air heated by an electric heater blowing on the aluminium alloy. A patent of Okada et al. [139] is the same as European Patent EP1462189B1 [140] and the Japanese patent JP2004291067A [141]. The researchers in [142,143] remarked that when forming AlMn1Mg1 aluminium, a tool with a flat tip produced better components formed by SPIF with different process conditions than a tool with a hemispherical tip in terms of formability, uniformity of thickness and the pillow effect, and the best geometric accuracy was obtained. Wei et al. [144] drew many conclusions from their experiment and simulation study of SPIF forming, such as that springback has an insignificant impact on the forming accuracy of the final part, and that there is a linear relationship between the wall angle and springback, i.e., a large wall angle of the formed part led to less springback. Sun et al. [145] studied the impact of ultrasonic vibration on the springback and surface quality of the AA-5052 aluminium alloy formed by SPIF. They found that forming sheets incrementally with ultrasonic assistance can reduce the springback effect. Rusu et al. [146] studied the behaviour of the following various aluminium alloys: AA 2007, EN AW 5754 and EN AW 6060 that were formed using SPIF, examining forming forces, thickness distribution and springback. The largest springback effect was seen in the AA 2007 alloy, which was accompanied by the lowest accuracy. Zhang et al. [147] investigated the effect of SPIF parameters on springback during forming assisted by ultrasonic vibration (UV). They found that a larger tool size led to greater springback, and that ultrasonic vibration reduced springback and improved geometric accuracy. Recently, artificial neural networks (ANN) have been employed with or without controlled manufacturing to develop efficient predictive models in many applications, including the metal forming process [148]. Various tool materials and shapes were examined to analyse the parametric factors that affect the geometric accuracy of AlMn1Mg1 components formed by SPIF. The results obtained were used to predict the accuracy in two different ANN models via two output neurons (Figure 10a) and one output neuron (Figure 10b) using a feed-forward neural network with a back propagation algorithm [149]. The SPIF process has been simulated by generating an elastoplastic finite element model (FEM), and the results obtained are compared to the experimental results of Han et al. [150]. The FEM results were adopted to predict springback using the ANNs.
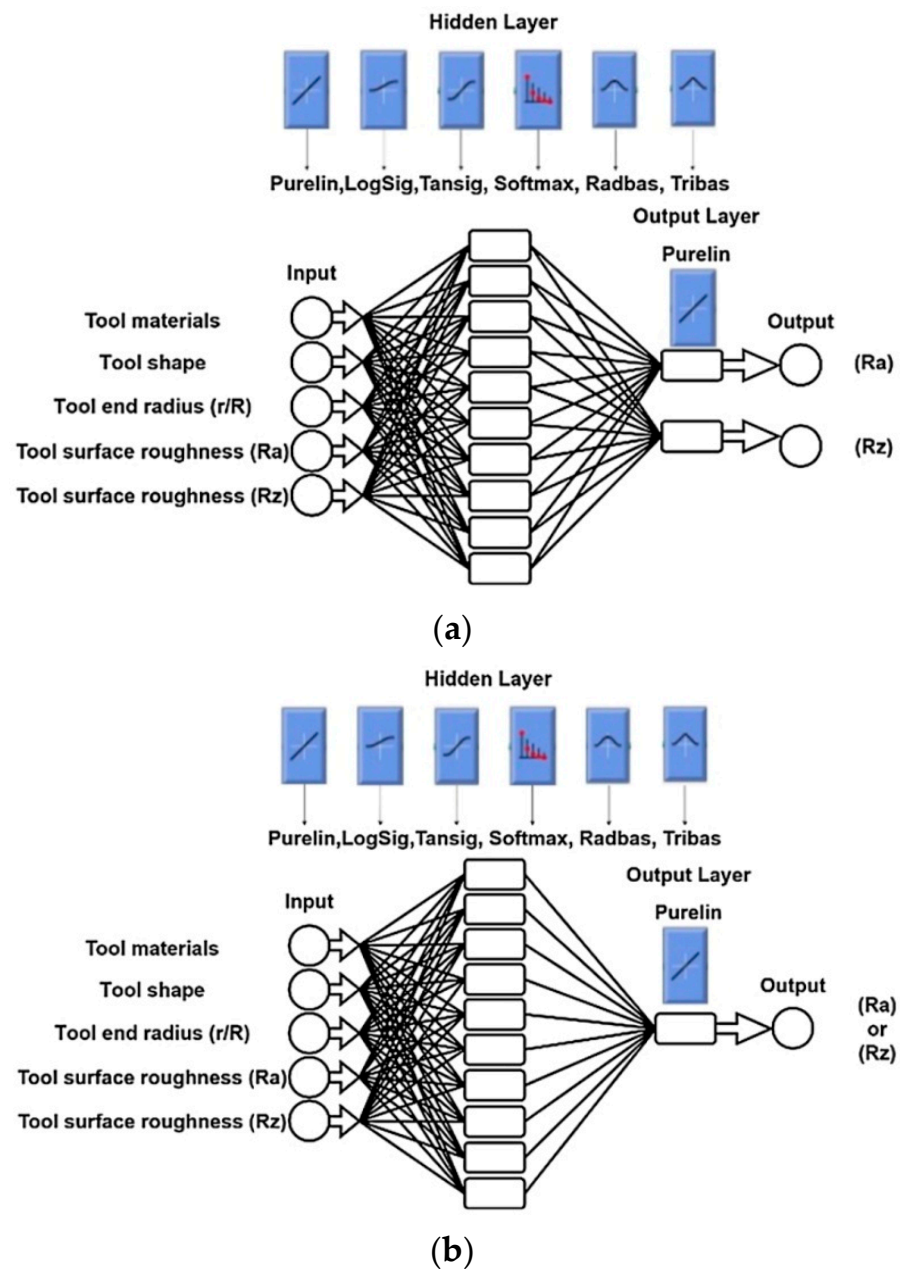
Figure 10. The ANN structure for modelling the effect of process parameters on the surface roughness of components: (**a**) two outputs, (**b**) one output (reprinted from [148]; copyright © 2022, The Authors, this is an open access article distributed under the terms of the Creative Commons CC BY license, which permits unrestricted use, distribution and reproduction in any medium, provided the original work is properly cited).

5.2. Toolpath Compensation

Dimensional deviation due to springback occurs between the geometry obtained and that desired at the end of the forming process and the release of the forming loads. Furthermore, different reasons lead to faulty components being formed by ISF. One of these is an inappropriate tool path. There are different tool path strategies used to form sheet metal in an incremental fashion. The two main tool paths used are spiral or contour paths. However, the forming tool moves peripherally along the programmed path in both types of tool path strategy. Jeswiet et al. [151] preferred the spiral path to the contour path despite the fact that the generation of a spiral path is more challenging than that of a contour one. Hirt et al. [152] assert that deviations in the geometry of components may happen in the

forming process even if the tool passes the selected path correctly and elastic deformation emerges during the process due to the local forming force; accordingly, the plastic deformation partly escapes from the formed sheet. There are the following two ways to control the geometric accuracy of components formed by ISF: tool path correction and optimisation of the process parameters. The disadvantages of SPIF components are the reduction in the geometric accuracy, especially the occurrence of the significant springback of the sheet; however, these can be minimised by algorithms for the correction of the tool path [36]. In various studies, the tool path in the ISF process has been modified to compensate for the springback value. The compensation process was adopted to achieve a more precise component. Related to what has been noted, Ambrogio et al. [153] studied the effect of incremental forming parameters on accuracy. They suggested a compensation scheme because sheet springback during the incremental forming process has an important influence on the forming accuracy. To this end, integration between the numerical and experimental procedures is introduced on AA1050-O. Hirt et al. [154] said that one can successfully form the part as designed by precisely following the tool path if all the deformations are totally pure plastic. Deviation can occur due to elastic deformation, and one of their suggested forming strategies increased the angle of the tool path from one stage to the next.

Feature-based tool path methods have been generated and compared with the conventional ISF tool path in three case studies by Lu et al. [155]. The new feature-based algorithm can obtain better geometric accuracy, particularly for non-symmetrical components without a supporting die. SPIF and counter SPIF, as the first and second stages of the incremental forming process, have been employed to decrease the springback of formed components and other shaping errors. If the tool path is not along the critical edge, tool marks may be left on the area where the tool path crosses the edge (Figure 11). The tool path of the second stage was developed on the basis of the first stage, while the first stage tool path was based on the part geometry.
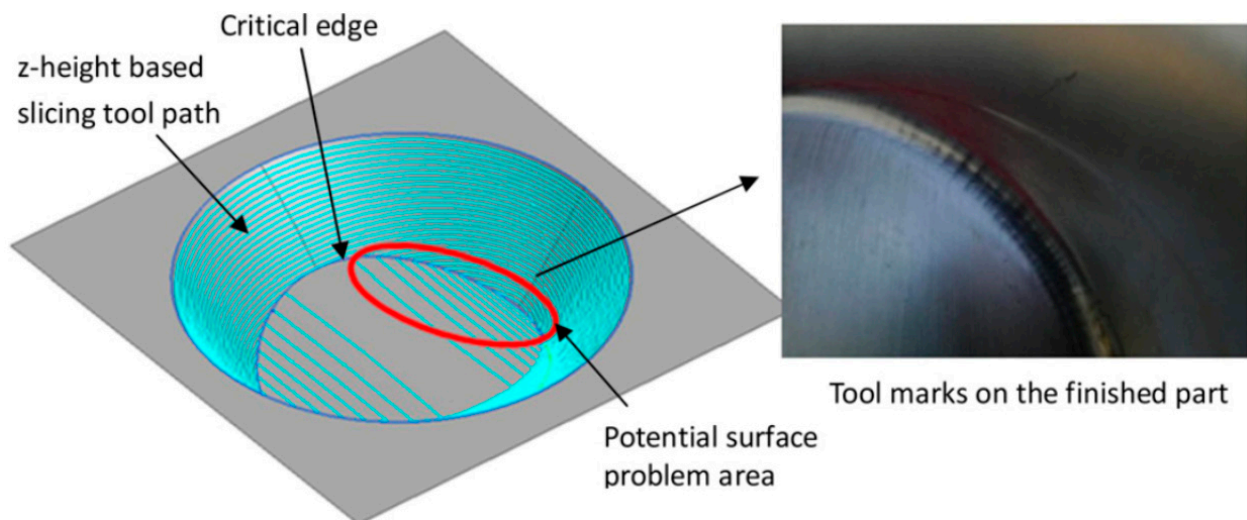

Figure 11. Potential surface problem in non-symmetrical part (reprinted with permission from [155]; copyright © 2022, Elsevier B.V. Published by Elsevier B.V. All rights reserved).

Jung et al. [156] used SPIF and counter SPIF as the first and second stages of the incremental forming process, which had been employed to decrease the springback of formed components and other shaping errors in the 5052 aluminium alloy. The tool path of the second stage was developed based on the first stage, while the first stage tool path was based on part geometry. Ren et al. [157] have generated a methodology suitable for arbitrary shapes and different ISF processes to reduce component inaccuracy, particularly in springback. The methodology developed mainly consists of the following three elements: finding

the critical key that affects the complexity of the geometry, offline simulation to predict springback and modifying the tool path in situ during the forming process (Figure 12).
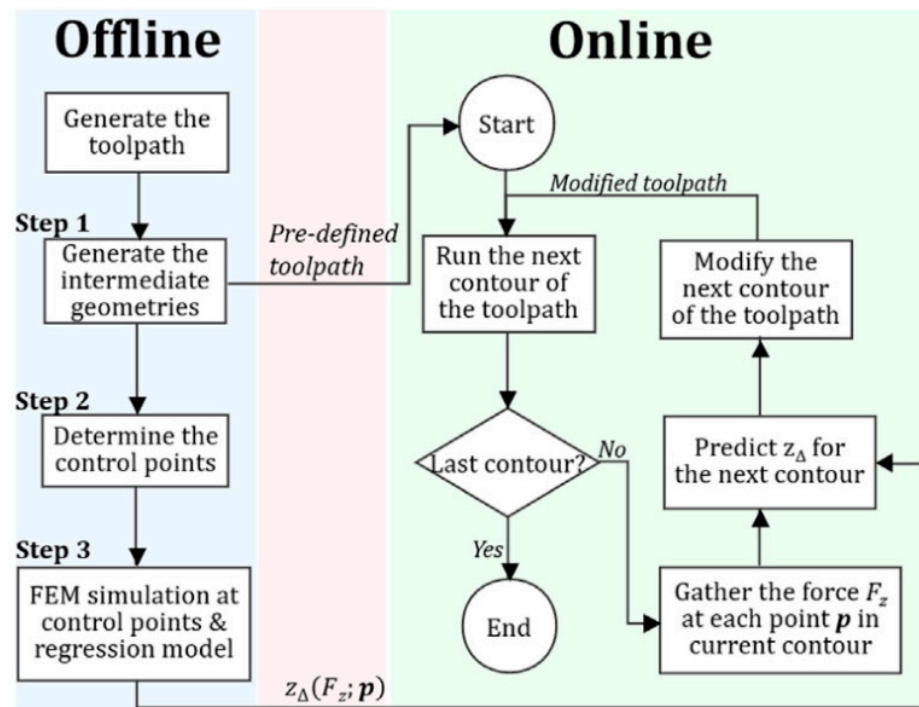

Figure 12. An in situ springback compensation method (reprinted with permission from [157]; copyright © 2022, Published by Elsevier Ltd. on behalf of CIRP).

By measuring the deviation between the ideal part and the part as formed, an algorithm was developed by Fiorentino et al. [158] to correct component geometry iteratively through the generation of a new, improved tool path. They eliminate the deviation to less than 0.4 mm in incrementally formed Al components. Rauch et al. [159] proposed a new method to generate and control Intelligent CAM (ICAM) tool paths. According to the process data assessment, this new approach modifies the tool paths during manufacturing using ISF. Behera et al. [160] presented a compensated tool path strategy as an error prediction to improve accuracy using multivariate adaptive regression splines (MARS). Fu et al. [161] developed an iterative closed-loop control algorithm in SPIF to correct the tool paths based on Fast Fourier and wavelet transforms. The springback of formed parts implemented by trial and corrected tool paths extracted from FEMs has been adopted in the algorithms developed.

5.3. Pillow Effect

The pillow effect is a concave surface occurring in the centre of the bottom of components, which is an undeformed area [162]. The pillow effect (bulge) is a significant manufacturing defect that negatively affects the geometric accuracy of parts formed using SPIF. Many studies have tried to find a proper method to stop the pillow effect occurring in parts formed by SPIF. The first observations on the pillow effect were made by Ambrogio et al. [163], who observed that besides the springback occurring after uploading, there was a sort of pillow effect (Figure 13) on the bottom base area. They noticed that the pillow effect was significantly affected by the tip diameter and part depth and there was an interaction between the factors mentioned and the wall angle.
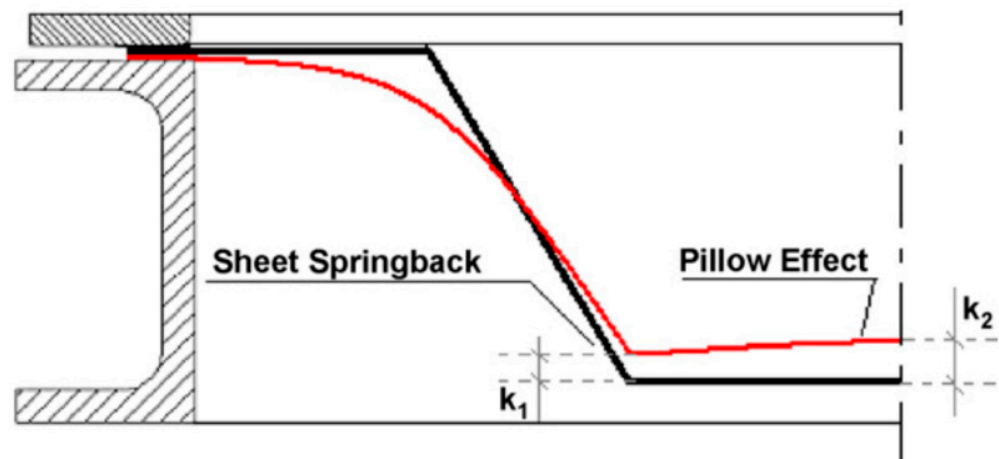
Figure 13. Schematic outline of the pillow effect (reprinted with permission from [163]; copyright © 2022, Elsevier B.V. All rights reserved).

Micari et al. [164] hinted that the reduced component accuracy of articles formed by ISF results from the following two typologies of error: springback in the wall and the pillow effect on the minor undeformed base. Isidore et al. [165] used Finite Element Analysis (FEA) for the prediction and control of the pillow effect in SPIF. Three-dimensional FEA and experiments were used to carry out incremental forming of aluminium 1050 and study the effect of different tool sizes and shapes. The results show that the use of a hemispherical tool produces strains and compressive stresses that generate the pillow effect due to the compression of the material. Flat tools reduce the pillow effect due to tensile stress and strains in the transverse direction. The pillow effect is more evident for thin geometries than for components formed at a maximum forming angle [166]. The pillow effect usually results in an increase in the forming forces, leading to more inaccuracies in the components. Zhang et al. [167] mentioned that work hardening in multi-point forming could reduce the pillow effect. The lower limit of the formability window of an AA1060-O part formed by SIPF was reduced due to the pillow effect, as unveiled by the experimental and FEA results [168]. Al-Ghamdi and Hussain [169] studied the mechanical properties of formed sheet metal on the pillow effect, and they found that a reduction in tensile fracture, which controls the sheet formability, does not have a noticeable effect on billowing. On the other hand, decreasing the property of the hardening exponent (controlling its influence on the stretchability of the metal) decreases the pillowing that is the most important property that influences the pillow effect. In addition, the pillow grows significantly with an increase in the forming depth, but not continuously; hence the pillow reduces at a specific depth due to the property of the hardening exponent. Afzal [170], however, stated that the formed part shows a pillow effect because the base of the sheet remains in the elastic state, while the rest of the sheet is in the plastic state. Essa and Hartley [171] examined different ways to increase the geometric accuracy of implementing FE in SPIF on the Al-5251-H22 aluminium alloy. They minimised the bending of the formed sheet by flanking a support plate, reducing springback by assigning a supporting tool and eliminating billowing by modifying the end stage of the tool path.

5.4. Thickness Distribution

Components produced by ISF have two main obstacles; thinning during forming and limited geometric accuracy. Thickness distribution/uniformity/homogeneity in ISF has become a critical issue, and several studies have been conducted in this area. It is worth mentioning that to overcome sheet thinning and improve thickness distribution, multi-stage forming strategies have been the approach typically used in ISF [61,151,154,172,173]. Nevertheless, it is still questionable which method can reduce thinning and how many forming stages are needed to obtain a uniform thickness distribution. To this end, based

on constant volume, Li et al. [174] suggested an equation to determine the appropriate number of forming stages required; moreover, they tested the rule they suggested by producing a complex product. Furthermore, they note that a more uniform distribution of sheet thickness in the double-forming process mainly results from an increase in the region undergoing total plastic deformation. Zhang et al. [167] developed multi-point forming to form the 2A12-O aluminium alloy as a primary step before starting the ISF process based on a thickness prediction model. A better thickness distribution was obtained as a result of the new method. Ambrogio et al. [175] conducted experimental and numerical research on pure aluminium, AA1050-O, to investigate the changes in the thickness distribution based on customised conditions imposed in SPIF. The approach was that by weakening the sheet from different positions, they found that the local deformation can be influenced by changing the strength of the sheet. Furthermore, the imposed weakening was helpful in reducing sheet strength, which helps to thin in an unweakened zone to produce a more uniform thickness distribution as the thinning is usually in the mid-zone in conventional SPIF. Utilising numerical models and experiments, Salem et al. [176] investigated the impact of the tool strain path on the formability and local thinning of AA7075-O sheets in SPIF. They revealed the following three different zones on the formed part wall: bending, thinning and steady-state, and they claimed that most of the thinning occurs under the tool. Azaouzi and Lebaal [49] optimised the forming strategy using FEA together with the response surface method (RMS) and sequential quadratic programming (SQP) algorithms. Their strategy improved the sheet thickness distribution of aluminium alloy by 7%. Awankar et al. [177] hinted that the thinning in the mid-zone of the sheet is because the material is encountering uniaxial stretching from both sides in this area. Zhu et al. [178] generated a new toolpath method to form straight wall components from 1060 aluminium sheets by multistage forming to eliminate the inhomogeneity in the thickness of the final product. In their method, the toolpath is based on parallel planes adopting a stretching angle to minimise the distance between the wall angle and the parallel planes. With insignificant warping at the bottom, the formed part's sidewall seems closer to the ideal shape by increasing the depth. However, in the ideal case without any thinning or excessive thickness, the sine law ($t = t_i \sin \theta$) can be helpful in predicting the end thickness of the part wall after forming. Where t is the final sheet thickness, t_i is the initial sheet thickness and θ is the wall angle of the formed part, and this has been used in many studies [179–182]. One can refer back to the sine law when considering shear spinning, as noted by Avitzur and Yang [183]. The sine law is a simple geometrical model for estimating sheet thickness in incremental sheet forming, which is not adequate and may supply only a rough and average approximation, and which, however, does not apply to all the regions along the final part wall because, as shown by Young and Jeswiet [184], sheet thinning does not always follow the sine law. Therefore, researchers proposed more practical and general ways to calculate sheet thickness [185,186]. Yang et al. [187] analysed the effects of SPIF parameters on the thinning ratio of a 1060 aluminium-formed part, both numerically and experimentally. Finally, a method was proposed to control the thinning rate by changing the forming trajectory. This method was closer to the actual values than those calculated using the sine law. However, the thinning rate increases with an increase in the tool tip diameter, wall angle and initial thickness, but decreases with an increase in step size. On the other hand, there was no mention of the influence of the feed rate on the thinning ratio. Cao et al. [188] compared the thickness distributions of items formed by SPIF and the results predicted for both the method developed, which tracked the nodal positions in each step-down, and the sine law. The authors assumed that the material point will move along its normal position on the surface in every transit time. Therefore, for any given point P on the final surface's $N+1$th level, the point position on the previous surface of the Nth level can be obtained by calculating the intersection point of the Ps and the profile curve of the Nth level (Figure 14). The method developed was more accurate than the sine law in predicting the thickness distribution of AA5052 and AA1100 aluminium alloys.
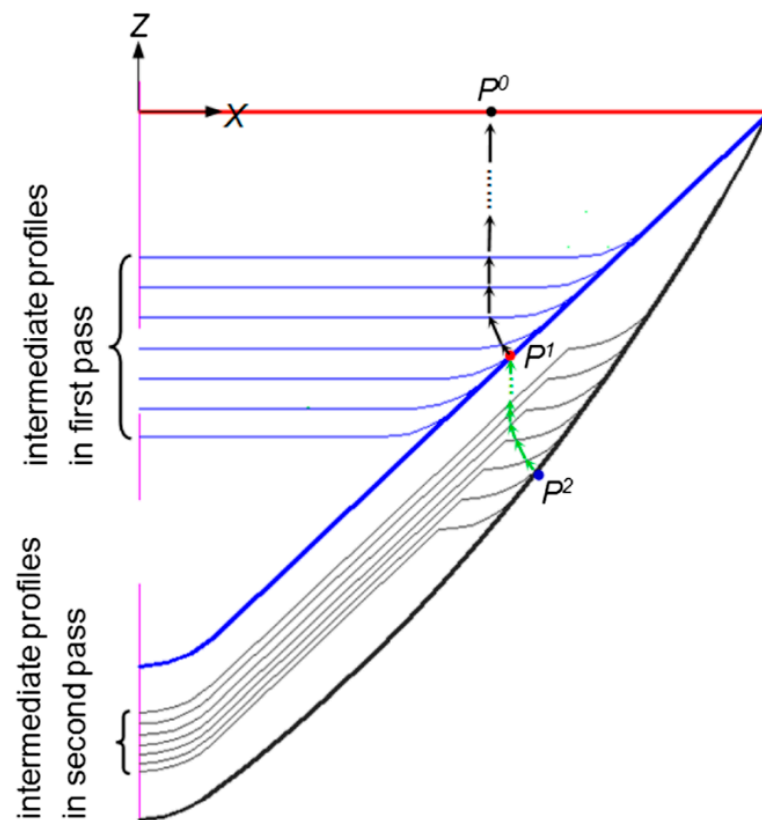
Figure 14. Schematic diagram of the pillow effect (reprinted with permission from [188]; copyright © 2022, Springer-Verlag London).

6. Surface Finish

6.1. Process Parameters

A significant problem occurring during the forming of aluminium and its alloys is galling, which significantly affects the quality of manufactured products, as well as reducing the durability of the tools [189,190]. However, the tribological properties of aluminium and its alloys, i.e., a high coefficient of friction, and the tendency to seize significantly limit their incremental forming, in which there are high contact pressures [191–193]. One of the ways to improve the surface quality of these sheets is to optimise the processing strategy, including the values of the processing parameters.

Surface finish or surface roughness is a main drawback in ISF, which limits the application of this process. The appropriate combination and optimisation of ISF parameters is a challenge and a critical concern [194]. To obtain an acceptable surface texture, it is important to control the process parameters (step size, tool rotation speed, forming angle, feed rate) and lubrication conditions. Thus, many papers have been devoted to studying the influences of these main factors on the final surface topography of the components that are subject to ISF. Azpen et al. [194] investigated the influence of step size, tool size, feed rate and tool rotation speed on the surface roughness of conical frustrums made from z6061-T6 aluminium alloy and formed using frictional stir incremental forming. The results of Taguchi's analysis have shown that tool diameter has a significant impact on the resulting internal surface roughness with a percentage contribution of 93.86%. Durante et al. [195] investigated the influence of the tool rotational speed and direction on the surface texture of the 7075-T0 aluminium alloy. When forming pyramidal frustums, roughness varies, but not considerably (Figure 15), depending on whether or not the tool is set in rotation, while neither the direction of rotation nor the tool rotational speed influence this parameter.
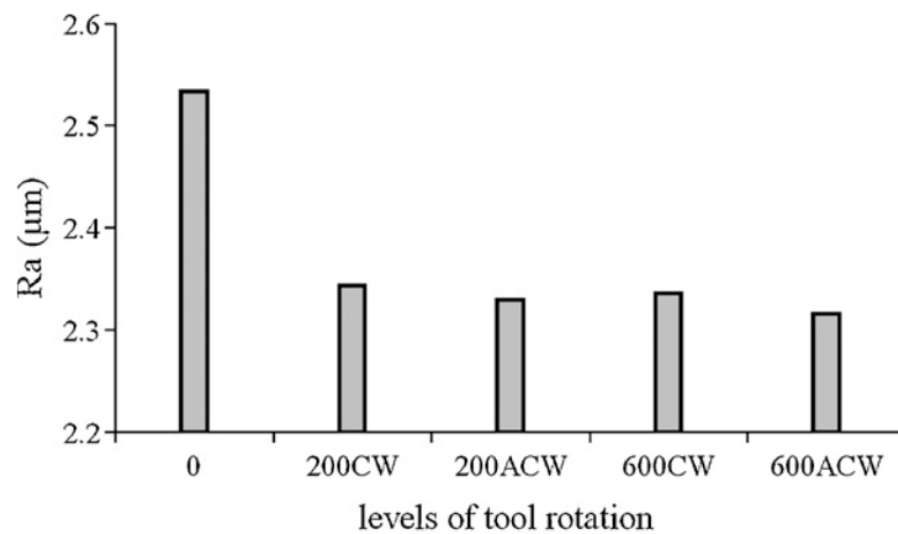
Figure 15. Roughness for different speeds of tool rotation (reprinted with permission from [195]; copyright © 2022, Elsevier B.V. All rights reserved).

Bhattacharya et al. [196] investigated the impact of tool size, step size and wall angle on the surface roughness of 5052 aluminium alloy sheets formed using ISF. The Box–Behnken method was used to design the experiments. The results of experiments showed that surface roughness decreases with an increase in the tool diameter and wall angle. The effects of forming at high feed rates and tool rotational speeds were studied by Hamilton and Jeswiet [197]. External non-contact surface roughness and the orange peel effect were studied when forming 3003-H14 aluminium alloy sheets. The model of surface characteristics that was developed based on the Design of Experiment (DoE) methodology can predict the orange peel effect and provide a good guide to enhancing the surface quality. Ambrogio et al. [198] experimentally investigated the incremental forming of truncated cones using a CNC lathe. The test materials were 1050-O aluminium and two 5754 and 6082-T6 aluminium alloy sheets with different thicknesses. It was found that the surface roughness is strongly influenced by the step size, sheet thickness and wall inclination angle. The feed rate had an insignificant impact. Lasunon et al. [199] used analysis of Variance (ANOVA) to study the effect of some factors on the surface finish of 5052-H32 aluminium alloy sheets. Their results proved that the interaction of step size and forming angle affected the surface texture that was achieved. The effect of feed rate can be neglected. Filice et al. [200] formed pyramidal frustums from 1050-O aluminium. It was found that the tool trajectory with constant step depth is unfavourable due to the surface finish produced. This strategy leaves marks at the end of each circle of the path, which produces a poor surface quality finish.

Liu et al. [201] studied the quantitative effects of sheet thickness, step down, tool diameter and feed rate on surface roughness using the response surface methodology with a Box–Behnken design. Forming investigations of 7075-T0 aluminium alloy sheets showed that sheet thickness is the most influential forming variable on the overall surface finish, followed by step down. Surface roughness was higher on the external non-contact surface than that of the internal tool-sheet contact surface. Mugendiran et al. [202] optimised the surface roughness and wall thickness of 5052 aluminium alloy drawpieces using a quadratic model with second order based on the feed rate, tool diameter and tool rotation. This study, based on Response Surface Methodology, is helpful in characterising the input variables in ISF. Lu et al. [203] used an oblique roller ball (ORB) to determine the impact of the tool design on the surface quality of four aluminium alloys named 1100, 2024, 5052 and 6111. The statistical analysis conducted confirmed that better surface roughness could be achieved with the new ORB tool (Figure 16) rather than the conventional tool. The

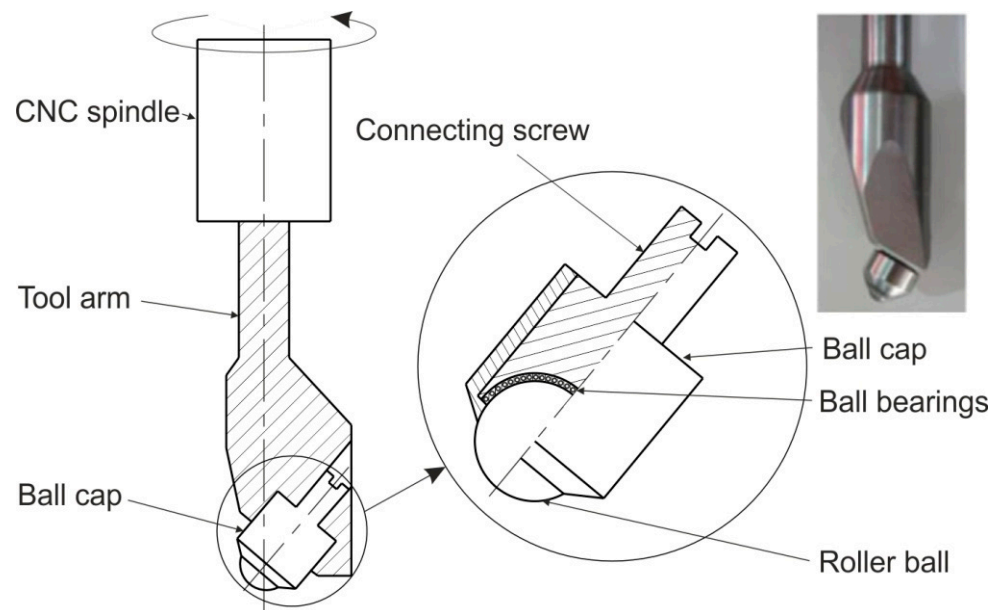advantages of the roller-based tool include better surface finish, higher formability and lower forming load.

Figure 16. The ORB tool (reprinted from [203], this is an open access article distributed under the terms of the Creative Commons CC-BY license, which permits unrestricted use, distribution and reproduction in any medium, provided the original work is properly cited).

Powers et al. [204] investigated the surface metrology in an SPIF of a 3003-O aluminium alloy. The effect of the sheet rolling mark direction on the surface topology in SPIF was studied, taking into consideration the forming direction and feed rate. They found that surface roughness Rz is greater with rolling marks perpendicular to the forming direction. Najm and Paniti [148] predicted the effects of forming tool characteristics on the surface roughness of AlMn1Mg1 aluminium foil formed using SPIF. Support Vector Regression (SVR) combined with artificial neural networks were used to predict the effects of process parameters on surface roughness. The effects of SPIF parameters on the surface roughness (Ra and Rz) of the formed sheet have been classified using Boosted Decision Trees. The classification is based on the importance of the parameter that causes the result of the surface roughness to fluctuate. The most important effect of the SPIF parameters on the sheet surface roughness Ra is the tool material and tool surface roughness Ra (Figure 17a). The ten-point roughness of a tool surface Rz has the most significant effect on the drawpiece surface roughness Rz (Figure 17b). The tool radius has the least effect on both of the surface roughness parameters considered.

Singh et al. [205] studied the effects of seven parameters at different levels of surface roughness of 2014 aluminium alloy components with three different thicknesses. They concluded that the feed rate, step size and tool path have little effect on surface roughness. However, the sheet thickness has an extreme effect on surface roughness. Mulay et al. [206] studied the effect of step size and feed rate on the surface roughness of 5754-H22 aluminium alloy drawpieces. They observed that the most significant parameter is step size, followed by feed rate. A slight increment in the step depth leads to a wavy surface finish. Nama et al. [207] found that surface roughness can be decreased during the SPIF of 1100 aluminium alloy sheets by increasing the feed rate, tool rotation speed and tool tip diameter.
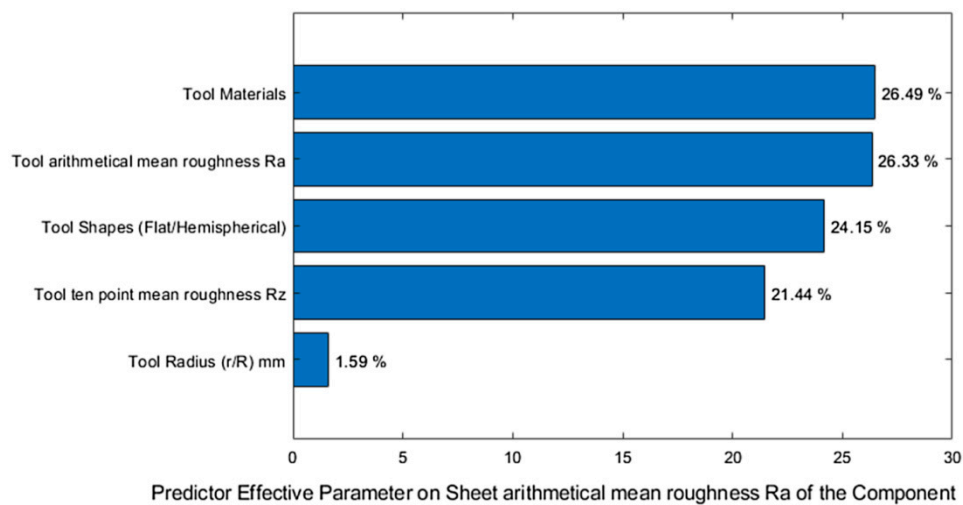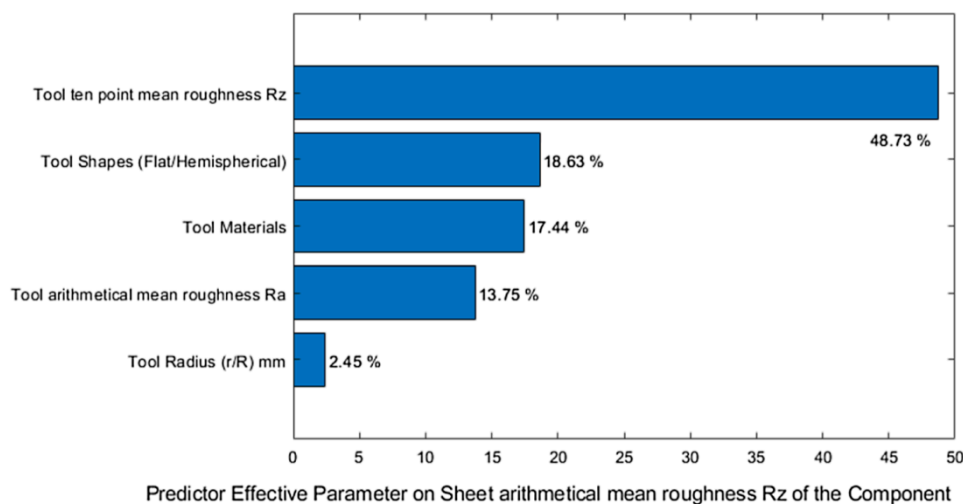
Figure 17. Effect of SPIF parameters on (**a**) the arithmetical mean roughness of the drawpiece surface Ra and (**b**) the ten point roughness of a drawpiece surface Rz (reprinted from [148]), this is an open access article distributed under the terms of the Creative Commons CC BY license, which permits unrestricted use, distribution and reproduction in any medium, provided the original work is properly cited.

6.2. Friction Conditions

High contact pressure, and consequently, the high levels of friction, in conventional ISF processes conducted in cold forming conditions may result in a poor surface finish. In friction-assisted ISF processes conducted in elevated temperatures, the high level of friction is a desirable phenomenon that allows the sheet to be heated to the required temperature. A detailed investigation of the friction effect is necessary for an improved sheet surface quality. Besides friction, the surface finish may be affected by the kind of both sheet and tool materials, lubrication conditions and processing parameters. Hagan and Jeswiet [208] characterised the surface finish of 3003 aluminium alloy drawpieces under different spindle speeds and depth increments. The results showed an exponential increase in the maximum peak-to-valley height as the increment size decreased. Hussain et al. [209] concluded that in order to ensure the presence of lubricant at the interface of the sheet and tool, a proper surface coating of the sheet-blank is an essential pre-requisite before forming. Moreover, they found that the surface quality is directly related to type of lubricant and lubrication method.

Friction is a major factor in contributing to the through-the-thickness-shear in the incremental forming process. Bambach et al. [210] observed the through-the-thickness-shear in the FE-based numerical simulation of 1050-H14 aluminium pyramids. It was found that the through-the-thickness-shear is dependent on both the vertical pitch and tool diameter. Eyckens et al. [211] investigated the effect of friction in the SPIF process when producing a large wall angle cone from an AA3103-O aluminium alloy sheet. They found that the through-the-thickness-shear was affected by the tool rotational speed.

In any forming process, the use of lubricants is essential at the interface between the workpiece and the tool. Lubricants improve heat distribution and give tools a longer life by reducing friction and wear [212,213]. Lubricants differ in many characteristics, such as consistency (i.e., fluid, paste, spray), density and viscosity. However, as concluded by Azevedo et al. [214], there is not much discussion in the literature about the differences between lubricants in relation to consumer choice. Suriyaprakan [215] found that AS-40 grease yielded good results when used in SPIF and the multistage ISF of 1050 aluminium alloy. Gulati et al. in [216] investigated the SPIF process for the 6063 aluminium alloy. The influential process parameters for surface roughness were identified using analysis of variance. They found that lubrication greatly affected the surface roughness compared to a dry process; therefore, they used a coolant lubricant for forming. Nama et al. [217] studied the ISF of 1100 aluminium sheets and found that the grease gave less surface roughness when compared with coolant oil in all cases. Najm and Paniti [148] successfully used machine oil when ISF forming AlMn1Mg0.5 sheets. Oraon and Sharma [217] used artificial neural networks to predict the surface finish of a component produced by the SPIF of the 3003-O aluminium alloy. The density of the lubricant is considered as one of the inputs. It was found that the average roughness parameter (Ra) is correlated with the density of the lubricant. Patel et al. [218] applied grey relational analysis to reduce the surface roughness of an SPIFed IS19000 aluminium sheet. They concluded that grease lubricant plays a vital role in incremental forming at a low spindle speed, whereas lubricating oil is preferred at a high spindle speed. Azevedo et al. [214] have studied lubrication considerations during the SPIF of steel or aluminium materials. Based on a literature study and the conclusion that there is a lack of information on the role played by the lubricant during the SPIF process, Azevedo et al. [214] tested the effect of several lubricants on the surface finish obtained using SPIF technology on 1050-T4 aluminium alloy sheets. It was concluded that it was possible to find a clear relationship between the viscosity of the lubricant used and the final roughness. Moreover, it was found that the greater the hardness of the blank material is, the lower the viscosity of lubricant necessary is. AL-M grease and SAE30 oil provided the best performance when forming 1050 aluminium alloy sheets.

The contact surface is small during SPIF and TPIF, and the forces during the forming process are low; therefore, the amount of lubricant required is reduced as compared to conventional SMF [129]. The ISF tool with lubrication does not leave scratches on the sheet and it is possible to associate the heating of the sheet with the friction. Duflou et al. [219] and Kim and Park [220] highlighted that the presence of lubricant is important during the SPIF of aluminium and Al-based alloys to avoid abrasive wear when the tool is relatively hard in comparison with the workpiece material.

In the case of hot ISF, molybdenum disulphide (MoS_2) is the most widely used lubricant. It is a solid inorganic compound used to reduce friction between the sheet and the tool. Usually, a thin layer of MoS_2 is brushed on the workpiece surface before forming [40]. The high temperature in hot ISF reduces the viscosity of a liquid lubricant, thereby adversely affecting its lubrication performance. At elevated temperatures, the use of high-performance lubricants allows one to overcome frictional effects [29]. Table 2 presents the typical lubricants used in the incremental sheet forming of aluminium and aluminium alloy sheets.

Table 2. Lubricants used in ISF of selected aluminium and Al-based alloys.

Lubricant	Workpiece Material	Conditions	Reference
MoS_2	AA2024-T3	hot forming	[40]
SAE 75W-85 gear oil	2024-T3 Alclad 7075-T6	cold forming	[32]
mineral oil	2219-O and 2219-T6	cold forming	[29]
without lubrication	3003	cold forming	[24]
without lubrication	1050	cold forming	[220]
oil	7075-T0	cold forming	[195]
10w30 servo oil	5754 H22	cold forming	[206]
machine oil	AlMgSi0.5	cold forming	[148]
Weicon AL-M paste	1050	cold forming	[214]
Moly Slip AS40 paste	1050	cold forming	[214]
oil	1050-O, 1050-H24, 6082	hot forming	[221]
mechanical oil	5052-H32	hot forming	[222]
Mineral oil (Total Finarol B 5746)	1050	cold forming	[214]
Moly Slip HSB paste	1050	cold forming	[214]
SAE 30 oil	1050	cold forming	[214]
Graphite powder + mineral oil (1:4)	7075-O	hot forming	[223]
SAE 0W-4	6061-T6	hot forming	[194]
water–oil emulsion cutting fluid	3003-H14	cold forming	[197]
graphite 33	5182	hot forming	[224]
solid lubricant (stick wax lubricant)	5052-H32	cold forming	[199]
MoS_2	5083	hot forming	[225]
MoS_2	5055	hot forming	[226]
without lubrication	1050	hot forming	[227]
graphite	6061	hot forming	[228]
solid graphite powder and lithium grease with scale 1:1	1050 H14	cold forming	[193]
20W-50	1050 H14	cold forming	[193]
machine oil	AlMn1Mg1 foil	cold forming	[142,143]
mineral oil	1050-O	cold forming	[185]
coolant oil, Gp Grease Calcium, Supergrees EP2, Zinol grease	AA1100	cold forming	[229]

7. Heat-Assisted Incremental Forming

Over almost two decades, there has been an intense development of warm forming processes as a response to limited ductility at room temperature. The elevated temperature of aluminium and aluminium alloys activates additional slip lines, allowing dislocations to take place [230]. It has been proven in tensile tests that an elevated temperature decreases the stress required for elongation [231]. The latest research focuses on the following three types of heat-assisted methods: electric hot incremental forming (EHIF), friction-stir-assisted incremental forming (FSIF) and laser-assisted incremental forming (LAIF). Although a source of heat is provided, in each method additional warmth is generated by friction between the tool and workpiece and as a result of the plastic deformation process.

7.1. Electrically Assisted ISF

There are a few variants of the electric heating arrangements: a heater located inside the tool or close to the sheet blank, or a direct current (DC) heating at the tool-workpiece contact point where the Joule effect $Q = R \times I^2 \times t$ (Q—the amount of heat released, I—electric current, R—electrical resistance of the conductor, t—current flow time) is used to increase the temperature by applying a high density current. A DC power source can be applied in two variants, connecting the anode to the forming tool and the cathode to the sheet causing local heating at the contact zone [40] or both electrodes only to the sheet as a part of a circuit, elevating the overall sheet temperature [226].

Hino et al. [225] were one of the first groups of researchers to arrange electric incremental forming in hard-to-form nonferrous metals. The authors positioned a 200 W heater and thermocouple inside the forming tool to achieve an elevated sheet temperature, mainly in the tool contact zone. That approach produced increased ductility, extended the forming limit and also reduced springback. Moreover, the possible limit angle of a cone formed from a 1-millimetre-thick EN AW 5083 sheet was increased from 50° to 75° by warming it up to 600 °C. Ambrogio et al. [40] applied a DC power source to a forming tool through attaching a graphite anode and a cathode directly to the sheet and locally warming up AA2024-T3 (Figure 18a). The determination of process workability windows and also the negative effects of electrical heating such as oxidation and reduced surface quality have been presented in their research. The authors highlighted that an increase in slope angle causes an increase in the energy delivered to the process.
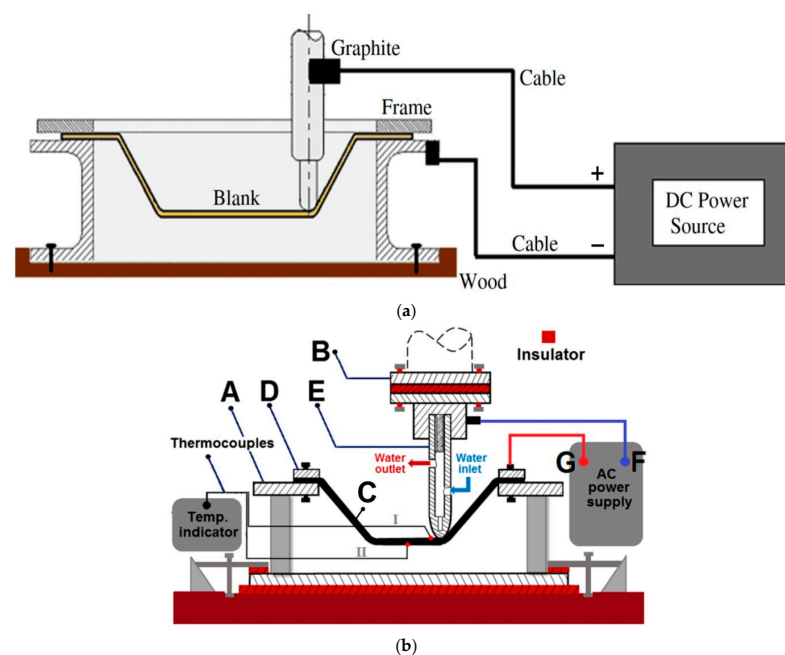

Figure 18. (**a**) Equipment for electrically assisted hot ISF (reprinted with permission from [40]; copyright © 2022, Elsevier Ltd. All rights reserved) and (**b**) the experimental equipment used in the experiments: A—base structure, B—tool holder, C—workpiece, D—blank holder, E—forming tool, F—Anode, G—cathode (reprinted with permission from [228]; copyright © 2022, Springer-Verlag London Ltd., part of Springer Nature).

Sy et al. [226] created a device with a global heating system for sheets by connecting both DC electrodes to the blank alone. Four thermocouples were welded to the bottom side of the formed sheet to control the circuit amperage in a closed loop. In a two-level factorial design, the authors noted that the elevated temperature allowed for the formation of an angle of up to 85° for AA5055, where the step size had the greatest impact on the surface roughness obtained. Moreover, the springback effect was reduced while the step size decreased. Li et al. [232] proved that the dimensional accuracy of Al1060 EHIF is

improved in comparison to Single-Stage Forming (SSF) and Double-Stage Forming (DSF) without a heat source. In a Box–Behnken design with response surface methodology, the authors studied the influence of input parameters such as tool diameter, feed rate, step size and DC current on the maximum, average and error (deviation between maximum and average) temperature, where the tool diameter seems to be the most significant factor in the experimental range.

Heating leads to lower forces and better formability but decreases the geometric accuracy caused by contraction; preheating the blank before forming allows deviations to be reduced by about 5%, which was proven in a numerical simulation presented by Pacheco and Silveira [233]. In further study [234], an investigation of the prediction of heat distribution using FEM analysis has been proposed using different variables (variants with/without convection and plastic strain) and shows a good agreement with the analytical model developed by Bejan et al. [235]. Singh et al. [227] conducted an incremental forming experiment with the following three ranges: room temperature, elevated both below and above the recrystallisation temperature of AA1050. Heaters located under a 1-millimetre-thick sheet warmed the whole sheet up. As a result, the forming temperature of 150 °C (below recrystallisation) produced the finest surface quality as well as the lowest reduction in drawpiece thickness. Vahdani et al. [228] applied the Taguchi method with analysis of variance to AA6061 EHISF. A forming device was used together with an AC transformer (Figure 18b) that was employed as the power supply with the output current in the range of 300–1000 A. Both electrodes were connected directly to the formed sheet. The tool diameter of Ø10 mm ended with a hemispherical radius of R = 5 mm and an additional internal tool cooling system was applied. Temperature indicators in the form of two thermocouples were located below the sheets. The amperage value was determined to be a key forming factor for AA6061 with a contribution of 73.6%. Selecting the optimal combination of the following process parameters: graphite lubricant; feed rate, 900 mm/min; step size, 0.2 mm; current, 300 A, achieved a 9.17-millimetre depth (9.14 mm was predicted by a model) before fracture, 1.12-micrometre Ra roughness parameter and a maximum sheet temperature of 95 °C with a tool wear of 0.14 mm.

In a study by Xiao et al. [231], ISF experiments were conducted with electric heaters located under the 1-millimetre-thick AA7075-T6 sheet and these were compared to FEM analysis. A variable temperature range of 20–200 °C, step size of 0.3–0.7 mm with a constant hemispherical tool diameter of Ø10 mm and feed rate of 200 mm/min were taken into consideration. The authors extended the forming limit angle from 50° to greater than 80° by warming up the blank from 20 to 200 °C in the Variable Wall Angle Cone Frustum (VWACF) test. FEM analysis prepared in ABAQUS/Explicit with the Kim-Tuan equation and with the Hill 1948 yield feature predicted the location of a fracture with high accuracy. Numerical and experimental investigations of SPIF assisted with cartridge heaters to heat the AA6061 were presented in a study by Darzi et al. [236]. The authors investigated the homogeneous warming of blanks in the temperature range 25–400 °C. By increasing the temperature to 400 °C, the height of a constant wall angle of 60° was increased from 7 to 44 mm until breakage and the critical angle was increased up to 65°. Further numerical simulations explained this effect by the reduced thinning caused by lower equivalent plastic strain. Copper-based anti-seize grease seems to be the favoured lubrication at 400 °C and the fracture depth was increased from 19.2 to 44 mm compared to the use of MoS_2 powder. If a higher temperature is used then there is better formability and lower forces are needed, but there is also a tendency to grain growth, which produces a drawpiece with decreased strength [237]. The vicinity of the fracture region features enhanced microhardness due to stretched and finer grains caused by stretching and the work hardening effect [84].

Rahmani et al. [238] proposed a novel method for expanding a tube by hot incremental forming where a ceramic circular heater warms up the blank. A 1.5-millimetre-thick AA6063 aluminium tube was used as a blank material. Their work focuses on the highest surface quality and formability by adjusting the temperature, the linear velocity of the tool and the axial and radial feed in a full factorial Design of Experiment (DoE). ANOVA shows

that temperature plays a key role in the bulge diameter (54.96% contribution) and final tube length (58.80% contribution), whereas the axial feed has a major impact on the surface roughness (57.23% contribution). The greatest expansion, 36.7%, was obtained at 300 °C.

Roth and Cao [133] patented electrically assisted double-sided incremental forming and the processes associated with it. In patent US8741079B2, dated 3 June 2014, the authors claimed a patent for sheet metal processing by double-sided incremental sheet forming DSISF while an electrical DC passes through it. In a further patent, no. WO2016/057688A1, Roth [137] claimed a method for springback reduction using electrically assisted manufacturing.

7.2. Friction-Assisted ISF

The easiest, and also a low-cost, way to generate local heat in the ISF process is provided by tool spinning. The amount of warmth depends mainly on the RPM value induced by the friction between the tool and the workpiece. Durante et al. [195] investigated the effects of tool rotation on AA7075-T0 forming. By measuring axial and radial forces, the friction coefficient was determined between the sheet and hemispherical steel punch. The authors achieved friction coefficients of $\mu = 0.19$ at 0 RPM, $\mu = 0.11$ at 200 and 400 RPM and $\mu = 0.06$ at 600 and 800 RPM. Further tests were conducted considering the clockwise and anticlockwise directions of the tool as well as selected tool rotation speeds of 0, 200 and 600 RPM. The sheet temperature level was measured by an attached thermocouple. A reduction in the horizontal and vertical forces was observed while the tool RPM increased and a minor improvement in surface roughness was caused by the rolling effect as opposed to sliding (at 0 RPM). The greater tool RPM affected the rise in temperature of the sheet. Hamilton and Jeswiet [197] studied the influence of forming parameters including high speeds of up to 2000 RPM and high feed rates of up to 8890 mm/min on the orange peel effect on the outer side of a 0.81-millimetre-thick AA3003-H14 drawpiece. In a full factorial design (DoE), step size was the most significant factor affecting the orange peel effect as well as grain size after forming. Buffa et al. [221] investigated local heating by the friction of AA1050-O, AA1050-H24 and AA6082-T6 sheets. The experiment resulted in a decrease in the average grain diameter and also in microhardness, while tool rotation rose to more than 4000 RPM. By these process parameters, the maximum wall angle was increased by an average of 10° as a result of dynamic recrystallisation.

Tool texturing effects have been investigated by Xu et al. [222]. Special rectangular oil pockets (Figure 19a) were created by a laser source on the hemispherical tip of the punch. This modification reduced the coefficient of friction between the tool and the sheet. However, as a consequence of the less heat generated, the formability decreased (with the same process parameters) when compared to the tool without texturing. Otsu et al. [239] observed a slightly wider formability in an advancing direction (tool rotation counter to feed direction) as well as a slightly improved drawpiece accuracy. Azpen et al. [194] found that a greater tool diameter causes an improvement in the inner surface roughness. The surface roughness parameter Ra on the inner surface (measured vertically and horizontally) was improved as the tool rotation increased; however, Gupta and Jeswiet [240] proved that an increase in the relative velocity between the tool and the workpiece has a marginal effect. Microhardness tests confirmed that at up to a 3000 RPM tool rotation, the sheet hardness increases due to the work hardening effect; beyond this limit there are decreases caused by the AA7075-O recrystallisation process [223]. Kumar et al. [107] observed an increase in formability, while the tool diameter or radius increased as well as the advantage of hemispherical tools over flat ends with a corner radius.

Riaz et al. [29] focused on comparing two temper conditions of AA2219 O (fully annealed) and T6 (solution heat treated and artificially aged). The authors applied the same tool RPM to both, and more heat was generated during forming in the T6 condition. This effect causes it to overheat and fracture at a depth of 25 mm, whereas the annealed state avoided this problem. Wang et al. [241] determined the process window by orthogonal analysis while forming AA2024-T3 and AA5052-H32 in terms of cutting and defects. To avoid the fish scale effect (Figure 19b), the feed rate to tool RPM ratio should be less than two. Zhan et al. [242] revealed the possibilities of the formation of microstructure and macroscopic properties during FS-ISF. AA2024 and AA6061 alloys were taken into account in their experiment. A process window was determined allowing one to customise the dislocation type, grain size and sub-grains and solute precipitates as well as better surface quality and elevated UTS and ductility by selecting the proper tool RPM and step size. Only dynamic recrystallisation and the consequential low-angle grain boundaries appeared due to the elevated temperature resulting from tool–sheet friction. Static recrystallisation is not possible because of the low residual temperature after processing [243].

Li et al. [244] proposed a novel approach to the process with, in addition, synchronous bonding. DC05 with an AA5052 sheet was stacked and formed simultaneously. Better formability and a lower bumping height on the stack centre were obtained for the steel top/aluminium bottom sequence with a climbing direction of forming (the direction of the feed rate was the same as the tool rotation at the contact zone) [245]. The process has been extended to the double-sided incremental forming variant [246]; the authors carried out a model predicting the bonding quality and they also reduced profile deviation by 3.8 mm compared to single point forming [247].

7.3. Laser-Assisted ISF

Laser assistance is the most expensive way to generate heat in the process, but at the same time, it is the most flexible, i.e., it allows the sheet to be warmed with an offset to the tool or to provide precise control of the size of the heated zone. It generally requires an additional independent CNC 3-axis with a laser source located below the formed sheet. Duflou et al. [224] investigated the laser-assisted incremental forming of AA5182 where the laser source was independently positioned on the opposite side of forming.

By setting a constant flow of coolant through the sheet, the temperature stabilised. An offset between the laser beam and forming tool was set to 2.4 mm and the spot size to 9 mm at a power of 160 W. An improvement in accuracy as well as a reduction in the force required and in the surface roughness Rz parameter was observed compared to cold forming.

In further work [248], a laser source has been used in the annealing process after cold SPIF as an alternative to LAISF and cold forming. It has been found that the laser annealing process does not affect the accuracy of drawpiece geometry; however, it reduces the work hardening effect. Lehtinen et al. [249] investigated an ISF experiment with 0.5-millimetre-thick AW-1050A and achieved a 61° wall angle with laser assistance compared to 59° with cold forming. Moreover, an additional laser source made an insignificant difference to the wall angle precision. That may be caused by the good formability of AW-1050A at room temperature and the low springback effect due to the low yield point. Mohammadi et al. [250] studied the influence of the laser position offset on AA5182-O sheet formability. High temperature isotherms wholly covering the contact zone are required to improve strain—a large laser beam without offset or large forward advance between the forming tool and workpiece is required. The authors noticed an enhanced formability because of the stress relief annealing effect. In further work [251], different sheet temper conditions were analysed and compared to the T-delivery state by LAISF. Investigations were carried out on test material consisting of 0.4-millimetre-thick AA2024 sheets in the following states: O-annealed, treatment and quenching with W-solution and heat treating, quenching and cold working with T-solution. A 41% improvement in formability for O-temper and 32% for W-temper were obtained in a cold forming process when compared to T-temper. The LAISF process, at about 360°C, affected the formability of T-state flows in a similar manner to O-state cold ISF, causing the maximum angle enhancement of 41% as well as, additionally, obtaining an accuracy improvement. A hardness improvement was observed, caused by partial particle dissolution during LAISF and consequent aging.

8. Conclusions

Incremental sheet forming is a promising technique for forming drawpieces with complex shapes that can be formed by the movement of a simple tool along a programmed path. The lack of a die makes this technique one of the most flexible in the metal forming industry. Many articles have been published in the field of conventional ISF and WJISF, the main purpose of which was to obtain components with a specific degree of deformation. At the same time, most of the authors studied the influence of several selected process parameters on the formability and surface finish of components. Although this article focuses on the current state-of-the-art in the scope of the ISF of aluminium and Al-based alloy sheets, most of the following conclusions also apply to the processing of other materials:

- The dieless nature of SPIF and TPIF greatly reduces the cost associated with making the dies required in conventional SMF processes. Changes can be made to the product design very quickly and easily, with minimal cost.
- A limitation of the industrial application of SPIF technique is that the forming time is much higher than in the conventional methods of sheet metal forming. After implementing a multi-point tool technique, it is possible to reduce the forming time drastically.
- The inner surfaces of the drawpieces are of low quality, which can be improved by the optimisation of the process parameters, especially step size and tool path strategy. New types of tool designs, i.e., an oblique roller ball tool, were developed to improve the surface finish of parts.
- By increasing the rotational speed of the tool, it is possible to increase the formability of the sheet material by friction-stir-assisted heating of the material.
- The presence of lubricant is important in the ISF of aluminium and Al-based alloys to avoid wear in the abrasive form when the tool is relatively hard in comparison with the workpiece material.
- The dimensional accuracy of an ISFed component may be improved by using different algorithms to optimise the tool path trajectory.
- Some Al-based alloys are included in the group of difficult-to-form materials. The formability of these alloys may be improved with methods of hot ISF. These methods include electrically assisted ISF, induction-heating-assisted ISF, laser-assisted ISF and combined electric- and friction-stir-assisted ISF.

- The use of modern variants of SPIF (i.e., ultrasonic-assisted ISF) permits a significant reduction in the manufacturing costs when forming "difficult-to-form" materials.
- Robotic ISF is more flexible than the CNC machine method, more cost-effective for large parts and easy to achieve when the right tools are used.
- The effect of step size in SPIF and TPIF is not unequivocal; some researchers have concluded that step size has a negative effect on formability; however, others have shown that step size does not affect formability.
- It is still hard to form parts with right angles or it cannot be achieved with one step. Parts with a 90° wall angle can be obtained by adopting non-linear strain paths by multi-stages, but to this end, the initial thickness of the sheet must be increased.
- The geometric accuracy attributed to and residual stresses and springback effects is one of the dominant limits for the further development of the ISF methods. There are the following two ways to reduce springback: (i) the use of an algorithm to compensate the elastic strains of the material after unloading and modifying the tool path strategy, and (ii) increasing the tool diameter and spindle speed and reducing the vertical step size.
- The surface roughness of the inner surface of an ISFed component may be improved by (i) reducing the tool size and vertical step size, and (ii) using a rotating tool as compared to a non-rotating one.
- There are no universal surface roughness parameters to describe the surface finish of SPIFed components. A more comprehensive parametric study can be beneficial to investigate the interdependence and interaction between forming parameters and surface roughness parameters of inner and outer surfaces of drawpieces.
- The parts produced by ISF have high surface roughness due to the waviness caused by the forming tool. When ISF is performed with a dummy sheet at the top of the main or target sheet, the surface roughness is minimized to some extent. In the SPIF process using a dummy sheet, two sheets are deformed simultaneously.
- Compared to traditional rigid tool incremental forming, water jet ISF has the following several advantages: no metallic contact between the tool and workpiece, environmental friendliness resulting from the absence of friction-reducing lubricants and a closed circuit for the working fluid and no tool wear during the forming process.
- It is suggested that future research should be focused on optimising process parameters for the use of SPIF methods to form various lightweight alloys used in the aerospace industry, in which products are manufactured in relatively small series.
- Finite element-based simulations can be used to predict forming defects, clarify the forming characteristics and improve the forming process. Accurate and efficient approaches for predicting the forming accuracy of drawpieces are awaited by the industrial designers of SPIF.
- There is little research on phenomenological or physical constitutive and damage models to describe the material behaviour of aluminium and aluminium alloy sheets. The effects of strain hardening and material anisotropy on the formability of hard-to-deform materials require further research.

Author Contributions: Conceptualization, T.T.; methodology, T.T.; validation, T.T., S.M.N., V.O., D.V., I.P. and M.S.; formal analysis, T.T., S.M.N., V.O. and I.P.; investigation, T.T., S.M.N., V.O., D.V., I.P. and M.S.; resources, T.T., S.M.N., V.O., D.V. and M.S.; data curation, T.T., S.M.N., V.O., D.V., I.P. and M.S.; writing—original draft preparation, T.T., S.M.N., V.O., D.V., I.P. and M.S.; writing—review and editing, T.T. All authors have read and agreed to the published version of the manuscript.

Institutional Review Board Statement: Not applicable.

Informed Consent Statement: Not applicable.

Data Availability Statement: The data presented in this study are available on request from the corresponding author.

Conflicts of Interest: The authors declare no conflict of interest.

References

1. Cheng, L.M.; Poole, W.J.; Embury, J.D.; Lloyd, D.J. The influence of precipitation on the work-hardening behavior of the aluminum alloys AA6111 and AA7030. *Metall. Mater. Trans.* **2003**, *34*, 2473–2481. [CrossRef]
2. Ubertalli, G.; Matteis, P.; Ferraris, S.; Marcianò, C.; D'Aiuto, F.; Tedesco, M.M.; De Caro, D. High Strain Rate Behavior of Aluminum Alloy for Sheet Metal Forming Processes. *Metals* **2020**, *10*, 242. [CrossRef]
3. Schneider, R.; Heine, B.; Grant, R.J.; Zouaoui, Z. Aluminium Sheet Metal Forming at Low Temperatures. *IOP Conf. Ser. Mater. Sci. Eng.* **2015**, *74*, 012014. [CrossRef]
4. Huber, G.; Djurdjevic, M.B.; Manasijevic, S. Determination some thermo-physical and metallurgical properties of aluminum alloys using their known chemical composition. *Int. J. Heat Mass Trans.* **2019**, *139*, 548–553. [CrossRef]
5. Taher, M.; Mao, F.; Berastegui, P.; Andersson, A.M.; Jansson, U. The influence of chemical and phase composition on mechanical, tribological and electrical properties of Silver-Aluminum alloys. *Tribol. Int.* **2018**, *119*, 680–687. [CrossRef]
6. Dudareva, N.; Gallyamova, R. The Cnfluence of Chemical Composition of Aluminum Alloys on the Quality of Oxide Layers Formed by Microarc Oxidation. *Mater. Today Proc.* **2019**, *11*, 89–94. [CrossRef]
7. Vijayakumar, M.D.; Dhinakaran, V.; Sathish, T.; Muthu, G.; Bupathiram, P.M. Experimental study of chemical composition of aluminium alloys. *Mater. Today Proc.* **2021**, *37*, 1790–1793. [CrossRef]
8. Ravikumar, R.N.; Rajesh, G.H. The mechanical properties and microstructure behavior of aluminium alloys subjected to shock waves. *Mater. Today Proc.* **2021**, *46*, 9132–9138. [CrossRef]
9. Hattori, C.S.; Almeida, G.F.C.; Gonçalves, R.L.C.; Santos, R.G.; Souza, R.C.; da Silva, W.C.; Cunali, J.R.C.; Couto, A.A. Microstructure and fatigue properties of extruded aluminum alloys 7046 and 7108 for automotive applications. *J. Mater. Res. Technol.* **2021**, *14*, 2970–2981. [CrossRef]
10. Garric, V.; Colas, K.; Donnadieu, P.; Loyer-Prost, M.; Leprêtre, F.; Cloute-Cazalaa, V.; Kapusta, B. Impact of the microstructure on the swelling of aluminum alloys: Characterization and modelling bases. *J. Nuclear Mater.* **2021**, *557*, 153273. [CrossRef]
11. Puga, H. Casting and Forming of Advanced Aluminum Alloys. *Metals* **2020**, *10*, 494. [CrossRef]
12. Dou, S.; Wang, X.; Xia, J.; Wilson, L. Analysis of Sheet Metal Forming (Warm Stamping Process): A Study of the Variable Friction Coefficient on 6111 Aluminum Alloy. *Metals* **2020**, *10*, 1189. [CrossRef]
13. Xiang, P.; Jia, L.J.; Shi, M.; Wu, M. Ultra-low cycle fatigue life of aluminum alloy and its prediction using monotonic tension test results. *Eng. Fract. Mech.* **2017**, *186*, 449–465. [CrossRef]
14. Zhao, X.; Li, H.; Chen, T.; Cao, B.; Li, X. Mechanical Properties of Aluminum Alloys under Low-Cycle Fatigue Loading. *Materials* **2019**, *12*, 2064. [CrossRef] [PubMed]
15. Shaha, S.K.; Czerwinski, F.; Kasprzak, W.; Friedman, J.; Chen, D.L. Improving High-Temperature Tensile and Low-Cycle Fatigue Behavior of Al-Si-Cu-Mg Alloys Through Micro-additions of Ti, V, and Zr. *Metall. Mater. Trans. A* **2015**, *46*, 3063–3078. [CrossRef]
16. EN 573-3:2019-12. *Aluminum and Aluminum Alloys-Chemical Composition and Types of Wrought Products-Part 3: Chemical Composition and Types of Articles*; European Committee For Standardization: Brussels, Belgium, 2019.
17. EN 1706:2020-10. *Aluminium and Aluminium Alloys. Castings. Chemical Composition and Mechanical Properties*; European Committee For Standardization: Brussels, Belgium, 2020.
18. Zheng, K.; Politis, D.J.; Wang, L.; Lin, J. A review on forming techniques for manufacturing lightweight complex—Shaped aluminium panel components. *Int. J. Light. Mater. Manuf.* **2018**, *1*, 55–80. [CrossRef]
19. Ismail, A.; Mohamed, M.S. Review on sheet metal forming process of aluminium alloys. In Proceedings of the 17th International Conference on Applied Mechanics and Mechanical Engineering, Cairo, Egypt, 19–21 April 2016; pp. 1–13.
20. Chen, J.; Lan, F.; Wang, J.; Wang, Y. Material Selection and Sheet Metal Forming Simulation of Aluminium Alloy Engine Hood Panel. In *Global Design to Gain a Competitive Edge*; Yan, X.T., Ion, W.J., Eynard, B., Eds.; Springer: London, UK, 2008; pp. 529–538.
21. Yahaya, S.N.M.; Ng, C.H.; Lai, C.F.; Sharrifuddin, S.; Grote, K.H. Reviews on the Forming Process of Heat Treatable Aluminium Alloys. *Int. J. Integr. Eng.* **2018**, *10*, 74–79. [CrossRef]
22. Jeswiet, J.; Geiger, M.; Engel, U.; Kleiner, M.; Schikorra, M.; Duflou, J.; Neugebauer, R.; Bariani, P.; Brushi, S. Metal forming progress since 2000. *CIRP J. Manuf. Sci. Technol.* **2008**, *1*, 2–17. [CrossRef]
23. Scholz, P.; Börner, R.; Kühn, R.; Müller, R. Dry Forming of Aluminium Sheet Metal: Influence of Different Types of Forming Tool Microstructures on the Coefficient of Friction. *Key Eng. Mater.* **2015**, *651–653*, 516–521. [CrossRef]
24. Jeswiet, J.; Hagan, E.; Szekeres, A. Forming parameters for incremental forming of aluminium alloy sheet metal. *Proc. Inst. Mech. Eng., Part B J. Eng. Manuf.* **2002**, *216*, 1367–1371. [CrossRef]
25. Meier, M.; Pfestorf, M.; Geiger, M.; Merklein, M. The use of dry film lubricants in aluminum sheet metal forming. *Wear* **2003**, *255*, 1455–1462.
26. Gronostajski, Z.; Pater, Z.; Madej, L.; Gontarz, A.; Lisiecki, L.; Łukaszek-Sołek, A.; Ziółkiewicz, S. Recent development trends in metal forming. *Arch. Civ. Mech. Eng.* **2019**, *19*, 898–941. [CrossRef]

27. Quadrini, F.; Santo, L.; Squeo, E.A. Flexible forming of thin aluminum alloy sheets. *Int. J. Modern. Manuf. Technol.* **2010**, *2*, 79–84.

28. Jaremenko, C.; Ravikumar, N.; Affronti, E.; Merklein, M.; Maier, A. Determination of Forming Limits in Sheet Metal Forming Using Deep Learning. *Materials* **2019**, *12*, 1051. [CrossRef]

29. Riaz, A.A.; Ullah, N.; Hussain, G.; Alkahtani, M.; Khan, M.N.; Khan, S. Experimental Investigations on the Effects of Rotational Speed on Temperature and Microstructure Variations in Incremental Forming of T6– Tempered and Annealed AA2219 Aerospace Alloy. *Metals* **2020**, *10*, 809. [CrossRef]

30. Behera, A.K.; Gu, J.; Lauwers, B.; Duflou, J.R. Influence of material properties on accuracy response surfaces in single point incremental forming. *Key Eng. Mater.* **2012**, *504*, 919–924. [CrossRef]

31. Bautista-Monsalve, F.; García-Sevilla, F.; Miguel, V.; Naranjo, J.; Manjabacas, M.C. A Novel Machine-Learning-Based Procedure to Determine the Surface Finish Quality of Titanium Alloy Parts Obtained by Heat Assisted Single Point Incremental Forming. *Metals* **2021**, *11*, 1287. [CrossRef]

32. Trzepieciński, T.; Kubit, A.; Dzierwa, A.; Krasowski, B.; Jurczak, W. Surface Finish Analysis in Single Point Incremental Sheet Forming of Rib-Stiffened 2024-T3 and 7075-T6 Alclad Aluminium Alloy Panels. *Materials* **2021**, *14*, 1640. [CrossRef]

33. Durante, M.; Formisano, A.; Langella, A. Observations on the influence of tool-sheet contact conditions on an incremental forming process. *J. Mater. Eng. Perform.* **2011**, *20*, 941–946. [CrossRef]

34. Ambrogio, G.; Filice, L.; Manco, G.L. Warm incremental forming of magnesium alloy AZ31. *CIRP Ann-Manuf Technol.* **2008**, *57*, 257–260. [CrossRef]

35. Ramulu, P.J. Aluminum Alloys Behavior during Forming. In *Aluminium Alloys and Composites*; Cooke, K., Ed.; IntechOpen Ltd.: London, UK, 2020; pp. 695–728.

36. Trzepieciński, T.; Oleksik, V.; Pepelnjak, T.; Najm, S.M.; Paniti, I.; Maji, K. Emerging Trends in Single Point Incremental Sheet Forming of Lightweight Metals. *Metals* **2021**, *11*, 1188. [CrossRef]

37. Sieniawski, J. Stopy aluminium stosowane w technice lotniczej. *Mechanik* **2009**, *7*, 649–654.

38. Djukanovic, G. Aluminium Alloys in the Automotive Industry: A Handy Guide. Available online: https://aluminiuminsider.com/aluminium-alloys-automotive-industry-handy-guide/ (accessed on 21 October 2021).

39. Kwiatkowski, L. Podatność na korozję i skuteczność aktualnych metod ochrony przed korozją stopów aluminium stosowanych w budownictwie. *Inżynieria Powierzchni* **2009**, *4*, 24–33.

40. Ambrogio, G.; Filice, L.; Gagliardi, F. Formability of lightweight alloys by hot incremental sheet forming. *Mater. Des.* **2012**, *34*, 501–508. [CrossRef]

41. Bao, W.; Chu, X.; Lin, S.; Gao, J. Experimental investigation on formability and microstructure of AZ31B alloy in electropulse-assisted incremental forming. *Mater. Des.* **2015**, *87*, 632–639. [CrossRef]

42. Dou, S.; Xia, J. Analysis of Sheet Metal Forming (Stamping Process): A Study of the Variable Friction Coefficient on 5052 Aluminum Alloy. *Metals* **2019**, *9*, 853. [CrossRef]

43. Sun, L.; Cai, Z.; He, D.; Li, L. Aluminum Alloy Sheet-Forming Limit Curve Prediction Based on Original Measured Stress-Strain Data and Its Application in Stretch-Forming Process. *Metals* **2019**, *9*, 1129. [CrossRef]

44. Xu, D.; Lu, B.; Cao, T.; Chen, J.; Long, H.; Cao, J. A comparative study on process potentials for frictional stir-and electric hot-assisted incremental sheet forming. *Procedia Eng.* **2014**, *81*, 2324–2329. [CrossRef]

45. Li, C.; Jiang, S.; Zhang, K. Pulse current-assisted hot-forming of light metal alloy. *Int. J. Adv. Manuf. Technol.* **2012**, *63*, 931–938. [CrossRef]

46. Preferred Reporting Items for Systematic Reviews and Meta-Analyses (PRISMA). Available online: http://prisma-statement.org/ (accessed on 10 October 2021).

47. Kumar, Y.; Kumar, S. Incremental Sheet Forming (ISF). In *Advances in Material Forming and Joining*; Narayanan, R.G., Dixit, U.S., Eds.; Springer: New Delhi, India, 2015; pp. 29–46.

48. Jackson, K.; Allwood, J. The mechanics of incremental sheet forming. *J. Mater. Process. Technol.* **2009**, *209*, 1158–1174. [CrossRef]

49. Azaouzi, M.; Lebaal, N. Tool path optimization for single point incremental sheet forming using response surface method. *Simul. Model. Pract. Theory* **2012**, *24*, 49–58. [CrossRef]

50. Selvam, A.J.M.; Velu, R.; Dheerankumar, T. Study of the Influence of the Process Variables on Formability and Strain Distribution in Incremental Sheet Metal Working of AA 1050 Sheets. In *Innovative Design and Development Practices in Aerospace and Automotive Engineering*; Bajpai, R., Chandrasekhar, U., Eds.; Springer: Singapore, 2014; pp. 493–505.

51. Leszak, E. Apparatus and Process for Incremental Dieless Forming. Patent No. US3342051A, 19 September 1967.

52. Berghan, W.G.; Murray, J.G.F. Method of Dielessly Forming Surfaces of Revolution. Patent No. US3316745A, 8 February 1965.

53. Berghan, W.G.; Murray, J.G.F. Process for the Production of Surfaces of Revolution. Patent No. DE1527973A1, 8 February 1965.

54. Emmens, W.C.; Sebastiani, G.; van den Boogaard, A.H. The technology of Incremental Sheet Forming—A brief review of the history. *J Mater. Process. Technol.* **2010**, *210*, 981–997. [CrossRef]

55. Mason, B. Sheet Metal Forming for Small Batches. Bachelor's Thesis, University of Nottingham, Nottingham, UK, 1978.

56. Appleton, E.; Mason, B. Sheet metal forming for small batches using sacrificial tooling. *Prod. Eng.* **1984**, *63*, 58. [CrossRef]

57. Matsubara, S. Incremental Backward Bulge Forming of a Sheet Metal with a Hemispherical Head Tool—A Study of a Numerical Control Forming System II. *J. Jpn. Soc. Technol. Plast.* **1994**, *35*, 1311–1316.

58. Oleksik, V.; Trzepieciński, T.; Szpunar, M.; Chodoła, Ł.; Ficek, D.; Szczęsny, I. Single-Point Incremental Forming of Titanium and Titanium Alloy Sheets. *Materials* **2021**, *14*, 6372. [CrossRef]

59. Trzepieciński, T.; Najm, S.M.; Sbayti, M.; Belhadjsalah, H.; Szpunar, M.; Lemu, H.G. New Advances and Future Possibilities in Forming Technology of Hybrid Metal–Polymer Composites Used in Aerospace Applications. *J. Compos. Sci.* **2021**, *5*, 217. [CrossRef]

60. Silva, M.B.; Martins, P.A.F. Two-Point Incremental Forming with Partial Die: Theory and Experimentation. *J. Mater. Eng. Perform.* **2013**, *22*, 1018–1027. [CrossRef]

61. Li, X.; Han, K.; Li, D. Multi-Stage Two Point Incremental Sheet Forming. *J. Phys Conf. Ser.* **2018**, *1063*, 012064. [CrossRef]

62. Iseki, H. A simple deformation analysis for incremental bulging of sheet metal using high speed water jet. In Proceedings of the 6th International Conference on Technology of Plasticity, Nuremberg, Germany, 19–24 September 1999; pp. 1483–1490.

63. Iseki, H. Flexible and incremental bulging of sheet metal using high–speed water jet. *JSME Int. J. Ser. C* **2001**, *44*, 468–493. [CrossRef]

64. Jurisevic, B.; Kuzman, K.; Junkar, M. Water jetting technology: An alternative in incremental sheet metal forming. *Int. J. Adv. Manuf. Technol.* **2006**, *31*, 18–23. [CrossRef]

65. Lu, B.; Bazeer, M.W.M.; Cao, J.F.; Ai, S.; Chen, J.; Ou, H.; Long, H. A study of incremental sheet forming by using water jet. *Int. J. Adv. Manuf. Technol.* **2017**, *91*, 2291–2301. [CrossRef]

66. Zhang, Q.; Zhang, T.T.; Lei, L.; Dai, M.Q. The high-pressure liquid jet incremental forming for the aluminum sheet. *Proc. Inst. Mech. Eng. Part B J. Eng. Manuf.* **2014**, *229*, 682–690. [CrossRef]

67. Emmens, W.C. Water jet forming of steel beverage cans. *Int. J. Mach. Tool. Manuf.* **2006**, *46*, 1243–1247. [CrossRef]

68. Jurisevic, B.; Sajn, V.; Kosel, F.; Junkar, M. Introduction of laminated supporting tools in water jet incremental sheet metal forming. *Int. J. Adv. Manuf. Technol.* **2008**, *37*, 496–503. [CrossRef]

69. Sajn, V.; Jurisevic, B.; Kosel, F. Water jet incremental sheet metal forming: Pressure distribution analysis. *Int. J. Interact. Des. Manuf.* **2011**, *5*, 95–102. [CrossRef]

70. Teymoori, F.; LohMousavi, M.; Etesam, A. Numerical analysis of fluid structure interaction in water jet incremental sheet forming process using coupled Eulerian–Lagrangian approach. *Int. J. Interact. Des. Manuf.* **2016**, *10*, 203–210. [CrossRef]

71. Kai, H.; Li, J.H.; Luo, Q.; Mao, H.; Du, R.X. A study on dieless incremental sheet metal forming using water jet technology. *Adv. Mater. Res.* **2011**, *189–193*, 795–800. [CrossRef]

72. Lu, B.; Cao, J.; Jun, C.; Bin, L.; Bin, L.; Jian, C.; Jun, C. High-Pressure Water Jet Plate Incremental Forming and Cutting Device. Patent No. CN102218706A, 24 March 2011.

73. He, K.; Li, J.; Mao, H.; Luo, Q.; Li, Q.; Kai, H.; Jiuhua, L.; He, M.; Qun, L.; Quanchang, L. High-Pressure Water Jet Flexible Incremental Forming Process and Device for Plates. Patent No. CN201110347675, 4 November 2011.

74. Psyk, V.; Kurka, P.; Kimme, S.; Werner, M.; Landgrebe, D.; Ebert, A.; Schwarzendahl, M. Structuring by electromagnetic forming and by forming with an elastomer punch as a tool for component optimisation regarding mechanical stiffness and acoustic performance. *Manuf. Rev.* **2015**, *2*, 23. [CrossRef]

75. Thibaudeau, E.; Kinsey, B.L. Analytical design and experimental validation of uniform pressure actuator for electromagnetic forming and welding. *J. Mater. Process. Technol.* **2015**, *215*, 251–263. [CrossRef]

76. Zhang, S.H.; Chen, S.F.; Ma, Y.; Song, H.W.; Cheng, M. Developments of new sheet metal forming technology and theory in China. *Acta Metall. Sin.* **2015**, *28*, 1452–1470. [CrossRef]

77. Long, A.; Wan, M.; Wang, W.; Wu, X.; Cui, X.; Ma, B. Forming methodology and mechanism of a novel sheet metal forming technology-electromagnetic superposed forming(EMSF). *Int. J. Solids Struct.* **2018**, *151*, 165–180. [CrossRef]

78. Psyk, V.; Risch, D.; Kinsey, B.L.; Tekkaya, A.E.; Kleiner, M. Electromagnetic forming—A review. *J. Mater. Process. Technol.* **2011**, *211*, 787–829. [CrossRef]

79. Kamal, M.; Shang, J.; Cheng, V.; Hatkevich, S.; Daehn, G.S. Agile manufacturing of a micro-embossed case by a two-step electromagnetic forming process. *J. Mater. Process. Technol.* **2007**, *190*, 41–80. [CrossRef]

80. Li, J.; Qiu, W.; Huang, L.; Su, H.; Tao, H.; Li, P. Gradient electromagnetic forming (GEMF): A new forming approach for variable-diameter tubes by use of sectional coil. *Int. J. Mach. Tools Manuf.* **2018**, *135*, 65–77. [CrossRef]

81. Yu, H.; Chen, J.; Liu, W.; Yin, H.; Li, C. Electromagnetic forming of aluminum circular tubes into square tubes: Experiment and numerical simulation. *J. Manuf. Process.* **2018**, *31*, 613–623. [CrossRef]

82. Centeno, G.; Martínez-Donaire, A.J.; Bagudanch, I.; Morales-Palma, D.; Garcia-Romeu, M.L.; Vallellano, C. Revisiting Formability and Failure of AISI304 Sheets in SPIF: Experimental Approach and Numerical Validation. *Metals* **2017**, *7*, 531. [CrossRef]

83. Cui, X.; Zhang, Z.; Yu, H.; Xiao, X.; Cheng, Y. Springback Calibration of a U-Shaped Electromagnetic Impulse Forming Process. *Metals* **2019**, *9*, 603. [CrossRef]

84. Feng, F.; Li, J.; Huang, L.; Liu, X.; Ma, H.; Li, G. The research of electromagnetic incremental forming process of Aluminum alloy sheet and the interaction between the die and the sheet. *Procedia Eng.* **2017**, *207*, 329–334. [CrossRef]

85. Cui, X.H.; Mo, J.H.; Li, J.J.; Zhao, J.; Zhu, Y.; Huang, L.; Li, Z.W.; Zhong, K. Electromagnetic incremental forming (EMIF): A novel aluminum alloy sheet and tube forming technology. *J. Mater. Process. Technol.* **2014**, *214*, 409–427. [CrossRef]

86. Imbert, J.M.; Winkler, S.L.; Worswick, M.J.; Oliveira, D.A.; Golovashchenko, S. The effect of tool–sheet interaction on damage evolution in electromagnetic forming of aluminum alloy sheet. *J. Eng. Mater. Technol.* **2005**, *127*, 145–153. [CrossRef]

87. Liu, X.; Huang, L.; Li, J.; Su, H. An electromagnetic incremental forming (EMIF) strategy for large-scale parts of aluminum alloy based on dual coil. *Int. J. Adv. Manuf. Technol.* **2019**, *104*, 411–431. [CrossRef]

88. Su, H.; Huang, L.; Li, J.; Ma, F.; Ma, H.; Huang, P.; Zhu, H.; Feng, F. Inhomogeneous deformation behaviors of oblique hole-flanging parts during electromagnetic forming. *J. Manuf. Process.* **2020**, *52*, 1–11. [CrossRef]

89. Guo, K.; Lei, X.; Zhan, M.; Tan, J. Electromagnetic incremental forming of integral panel under different discharge conditions. *J. Manuf. Process.* **2017**, *28*, 373–382. [CrossRef]

90. Trzepieciński, T. Recent Developments and Trends in Sheet Metal Forming. *Metals* **2000**, *10*, 779. [CrossRef]

91. Balanethiram, V.S.; Hu, X.; Altynova, M.; Daehn, G.S. Hyperplasticity: Enhanced formability at high rates. *J. Mater. Process. Technol.* **1994**, *45*, 595–600. [CrossRef]

92. Golovashchenko, S.F. Material formability and coil design in electromagnetic forming. *J. Mater. Eng. Perform.* **2007**, *16*, 314–320. [CrossRef]

93. Neto, D.M.; Martins, J.M.P.; Oliveira, M.C.; Menezes, L.F.; Alves, J.L. Evaluation of strain and stress states in the single point incremental forming process. *Int. J. Adv. Manuf. Technol.* **2016**, *85*, 521–534. [CrossRef]

94. Shrivastava, P.; Tandon, P. Microstructure and texture based analysis of forming behavior and deformation mechanism of AA1050 sheet during Single Point Incremental Forming. *J. Mater. Process. Technol.* **2019**, *266*, 292–310. [CrossRef]

95. Barnwal, V.K.; Chakrabarty, S.; Tewari, A.; Narasimhan, K.; Mishra, S.K. Forming behavior and microstructural evolution during single point incremental forming process of AA-6061 aluminum alloy sheet. *Int. J. Adv. Manuf. Technol.* **2018**, *95*, 921–935. [CrossRef]

96. Ai, S.; Dai, R.; Long, H. Investigating formability enhancement in double side incremental forming by developing a new test method of tension under cyclic bending and compression. *J. Mater. Process. Technol.* **2020**, *27*, 116349. [CrossRef]

97. Ingarao, G.; Zaheer, O.; Campanella, D.; Fratini, L. Re-forming end-of-life components through single point incremental forming. *Manuf. Lett.* **2020**, *24*, 132–135. [CrossRef]

98. Do, V.C.; Nguyen, D.T.; Cho, J.H.; Kim, Y.S. Incremental forming of 3D structured aluminum sheet. *Int. J. Precis. Eng. Manuf.* **2016**, *17*, 217–223. [CrossRef]

99. Abd Ali, R.; Chen, W.; Jin, K.; Bao, Y.; Hussein, A.W. Formability and failure analyses of Al/SUS bilayer sheet in single point incremental forming. *Int. J. Adv. Manuf. Technol.* **2019**, *105*, 2785–2798. [CrossRef]

100. Jeswiet, J.; Young, D. Forming limit diagrams for single-point incremental forming of aluminium sheet. *Proc. Inst. Mech. Eng. Part B J. Eng. Manuf.* **2005**, *219*, 359–364. [CrossRef]

101. Mugendiran, V.; Gnanavelbabu, A. Comparison of FLD and thickness distribution on AA5052 aluminium alloy formed parts by incremental forming process. *Procedia Eng.* **2014**, *97*, 1983–1990. [CrossRef]

102. Madeira, T.; Silva, C.M.A.; Silva, M.B.; Martins, P.A.F. Failure in single point incremental forming. *Int. J. Adv. Manuf. Technol.* **2015**, *80*, 1471–1479. [CrossRef]

103. Kumar, G.; Maji, K. Investigations into Enhanced Formability of AA5083 Aluminum Alloy Sheet in Single-Point Incremental Forming. *J. Mater. Eng. Perform.* **2021**, *30*, 1289–1305. [CrossRef]

104. Alinaghian, I.; Ranjbar, H.; Beheshtizad, M.A. Forming Limit Investigation of AA6061 Friction Stir Welded Blank in a Single Point Incremental Forming Process: RSM Approach. *Trans. Indian Inst. Met.* **2017**, *70*, 2303–2318. [CrossRef]

105. Carlone, P.; Thuillier, S.; Andrade-Campos, A.; de Sousa, R.J.A.; Valente, R. Incremental forming of friction-stir welded aluminium blanks: An integrated approach. *Int. J. Mater. Form.* **2021**, *14*, 1121–1137. [CrossRef]

106. Buffa, G.; Gucciardi, M.; Fratini, L.; Micari, F. Multi-directional vs. mono-directional multi-step strategies for single point incremental forming of non-axisymmetric components. *J. Manuf. Processes* **2020**, *55*, 22–30. [CrossRef]

107. Kumar, A.; Gulati, V.; Kumar, P.; Singh, V.; Kumar, B.; Singh, H. Parametric Effects on Formability of AA2024-O Aluminum Alloy Sheets in Single Point Incremental Forming. *J. Mater. Res. Technol.* **2019**, *8*, 1461–1469. [CrossRef]

108. Baruah, A.; Pandivelan, C.; Jeevanantham, A.K. Optimization of AA5052 in incremental sheet forming using grey relational analysis. *Measurement* **2017**, *106*, 95–100. [CrossRef]

109. Ebrahimzadeh, P.; Baseri, H.; Mirnia, M.J. Formability of aluminum 5083 friction stir welded blank in two-point incremental forming process. *Proc. Inst. Mech. Eng. Part E J. Process Mech. Eng.* **2018**, *232*, 267–280. [CrossRef]

110. Vanhove, H.; Mohammadi, A.; Duflou, J.R. Incremental forming of aluminium alloys in cryogenic environment. *AIP Conf. Proc.* **2016**, *1769*, 070020. [CrossRef]

111. Yang, M.; Bai, L.; Li, Y.; Yuan, Q. Influences of Vibration Parameters on Formability of 1060 Aluminum Sheet Processed by Ultrasonic Vibration-Assisted Single Point Incremental Forming. *Adv. Mater. Sci. Eng.* **2019**, *2019*. [CrossRef]

112. Callebaut, B.; Duflou, J.; Verbert, J. Asymmetric Incremental Sheet Forming System. Patent No. US7984635B2, 26 July 2011.

113. Ren, F.; Xia, Z.C. Method to Improve Geometrical Accuracy of an Incrementally Formed Workpiece. Patent No. US8783078B2, 22 July 2014.

114. Ren, F.; Xia, Z. The Method of Gradually Forming the Workpiece. Patent No. CN102343386A, 8 February 2012.

115. Ren, F.; Xia, Z.C. Verfahren Zum Verbessern Der Geometrischen Genauigkeit Eines Inkrementell Ausgebildeten Werkstücks. Patent No. DE102011079734A1, 10 May 2012.

116. Ren, F.; Xia, Z.C. Method of Geometric Accuracy Increasing of Part Produced by Incremental Formation. Patent No. RU2576792C2, 10 March 2016.

117. Johnson, C.F.; Kiridena, V.S.; Ren, F.; Cedric, Z. System and Method for Incrementally Forming a Workpiece. Patent No. US8322176B2, 4 December 2012.

118. Johnson, C.F.; Vigeda, S.K.; Ren, F.; Xia, Z. System for Progressively Forming Workpieces. Patent No. CN201744547U, 16 February 2011.

119. Janos, S.; Paniti, I. Device for Two Sided Incremental Sheet Forming. Patent No. EP2505279A1, 3 October 2012.

120. Roth, J.T.; Grimm, T.J.; Craig, G. Incremental Forming Tools and Method. Patent No. US11072015B2, 27 July 2021.

121. Roth, J.T.; Grimm, T.J.; Craig, G. New Incremental Forming Tools and Method. Patent No. US62311689, 22 March 2017.

122. Cao, J.; Malhotra, R. System and Method for Accumulative Double Sided Incremental Forming. Patent No. US9168580B2, 27 October 2015.

123. Cao, J.; Malhotra, R. System and Method for Accumulative Double Sided Incremental Forming. Patent No. WO2013062827A1, 2 May 2013.

124. Konka, P.; Nallagundla, V.R.; Prakash, O.; Sahu, M. Tool for Enhanced Accuracy in Double-Sided Incremental Forming. Patent No. US20210237140A1, 5 August 2021.

125. Konka, P.; Nallagundla, V.R.; Prakash, O.; Sahu, M. A Tool for Improved Accuracy in Double-Sided Incremental Forming. Patent No. EP3858511A1, 5 January 2021.

126. Konka, P.; Nallagundla, V.R.; Prakash, O.; Sahu, M. A Tool for Improved Accuracy in Double-Sided Incremental Forming. Patent No. CN113198919A, 15 November 2020.

127. Kiridena, V.S.; Xia, Z.C.; Ren, F. High Stiffness and High Access Forming Tool for Incremental Sheet Forming. Patent No. US8021501B2, 19 May 2016.

128. Edwards, W.L.; Grimm, T.J.; Ragai, I.; Roth, J.T. Optimum Process Parameters for Springback Reduction of Single Point Incrementally Formed Polycarbonate. *Procedia Manuf.* **2017**, *10*, 329–338. [CrossRef]

129. Gatea, S.; Ou, H.; McCartney, G. Review on the influence of process parameters in incremental sheet forming. *Int. J. Adv. Manuf. Technol.* **2016**, *87*, 479–499. [CrossRef]

130. Bambach, M.; Taleb Araghi, B.; Hirt, G. Strategies to improve the geometric accuracy in asymmetric single point incremental forming. *Prod. Eng.* **2009**, *3*, 145–156. [CrossRef]

131. Liu, Y.C. Method of Reducing Springback in Mechanically Pressed Sheet Materials. Patent No. EP0055435A2A, 18 December 1981.

132. Liu, Y.C. Method of Reducing Springback in Mechanically Pressed Sheet Materials. Patent No. US4373371A, 15 February 1983.

133. Roth, J.; Cao, J. Electrical-Assisted Double Side Incremental Forming and Processes Thereof. Patent No. US8741079B2, 3 June 2014.

134. Roth, J.; Cao, J. Electrical-Assisted Double Side Incremental Forming and Processes Thereof. Patent No. WO2012030835A2, 8 March 2012.

135. Roth, J.T. Single Point Incremental Forming of Metallic Materials using Applied Direct Current. Patent No. US8021501B2, 20 September 2011.

136. Roth, J.T. Method for Reducing Springback Using Electrically-Assisted Manufacturing. Patent No. US10500629B2, 10 December 2019.

137. Roth, J.T. Method for Reducing Springback Using Electrically-Assisted Manufacturing. Patent No. WO2016057688Al, 14 April 2016.

138. Roth, J.; Cao, J. Apparatus for Electrically Assisted Incremental Forming and Process Thereof. Patent No. US9951397B2, 25 June 2018.

139. Okada, N.; Ro, G.; Suzuki, Y. Method and Apparatus for Incremental Forming. Patent No. US6971256B2, 6 December 2005.

140. Okada, N.; Ro, G.; Suzuki, Y. Method and Apparatus for Incremental Forming. Patent No. EP1462189B1, 29 September 2004.

141. Okada, N.; Ro, G.; Suzuki, Y. Method and Apparatus for Incremental Forming. Patent No. JP2004291067A, 21 October 2004.

142. Najm, S.M.; Paniti, I. Study on Effecting Parameters of Flat and Hemispherical end Tools in SPIF of Aluminium Foils. *Teh. Vjesn.-Tech. Gaz.* **2020**, *27*, 1844–1849.

143. Najm, S.M.; Paniti, I. Experimental Investigation on the Single Point Incremental Forming of AlMn1Mg1 Foils using Flat End Tools. *IOP Conf. Ser. Mater. Sci. Eng.* **2018**, *448*, 012032. [CrossRef]

144. Wei, H.; Zhou, L.; Heidarshenas, B.; Ashraf, I.K.; Han, C. Investigation on the influence of springback on precision of symmetric-cone-like parts in sheet metal incremental forming process. *Int. J. Light. Mater. Manuf.* **2019**, *2*, 140–145. [CrossRef]

145. Sun, Y.; Lu, Z.; Li, C.; Wang, R.; Zhai, W. Study on the Springback Effect and Surface Property for Ultrasonic-Assisted Incremental Sheet Forming of Aluminum Alloy. *Symmetry* **2021**, *13*, 1217. [CrossRef]

146. Rusu, G.P.; Bârsan, A.; Popp, M.O.; Maroșan, A. Comparison between aluminum alloys behavior in incremental sheet metal forming process of frustum pyramid shaped parts. *IOP Conf. Ser. Mater. Sci. Eng.* **2021**, *1009*, 012054. [CrossRef]

147. Zhang, L.; Wu, C.; Sedaghat, H. Ultrasonic vibration–assisted incremental sheet metal forming. *Int. J. Adv. Manuf. Technol.* **2021**, *114*, 3311–3323. [CrossRef]

148. Najm, S.M.; Paniti, I. Predict the Effects of Forming Tool Characteristics on Surface Roughness of Aluminum Foil Components Formed by SPIF Using ANN and SVR. *Int. J. Precis. Eng. Manuf.* **2021**, *22*, 13–26. [CrossRef]

149. Najm, S.M.; Paniti, I. Artificial neural network for modeling and investigating the effects of forming tool characteristics on the accuracy and formability of thin aluminum alloy blanks when using SPIF. *Int. J. Adv. Manuf. Technol.* **2021**, *114*, 2591–2615. [CrossRef]

150. Han, F.; Mo, J.; Qi, H.; Long, R.; Cui, X.; Li, Z. Springback prediction for incremental sheet forming based on FEM-PSONN technology. *Trans. Nonferrous Met. Soc. China* **2013**, *23*, 1061–1071. [CrossRef]

151. Jeswiet, J.; Micari, F.; Hirt, G.; Bramley, A.; Duflou, J.; Allwood, J. Asymmetric single point incremental forming of sheet metal. *CIRP Ann.–Manuf. Technol.* **2005**, *54*, 88–114. [CrossRef]

152. Hirt, G.; Kordtomeikel, R.; Bremen, T.; Laugwitz, M.; Bailly, D. On the Geometrical Accuracy in Incremental Sheet Forming. In *Forming the Future. The Minerals, Metals & Materials Series*; Daehn, G., Cao, J., Kinsey, B., Tekkaya, E., Vivek, A., Yoshida, Y., Eds.; Springer: Cham, Switzerland; pp. 507–521.

153. Ambrogio, G.; Costantino, I.; de Napoli, L.; Filice, L.; Fratini, L.; Muzzupappa, M. Influence of some relevant process parameters on the dimensional accuracy in incremental forming: A numerical and experimental investigation. *J. Mater. Process. Technol.* **2004**, *153*, 501–507. [CrossRef]

154. Hirt, G.; Ames, J.; Bambach, M.; Kopp, R.; Kopp, R. Forming strategies and Process Modelling for CNC Incremental Sheet Forming. *CIRP Ann.* **2004**, *53*, 203–206. [CrossRef]
155. Lu, B.; Chen, J.; Ou, H.; Cao, J. Feature-based tool path generation approach for incremental sheet forming process. *J. Mater. Process. Technol.* **2013**, *213*, 1221–1233. [CrossRef]
156. Jung, K.S.; Yu, J.H.; Chung, W.J.; Lee, C.W. Tool Path Design of the Counter Single Point Incremental Forming Process to Decrease Shape Error. *Materials* **2020**, *13*, 4719. [CrossRef]
157. Ren, H.; Xie, J.; Liao, S.; Leem, D.; Ehmann, K.; Cao, J. In-situ springback compensation in incremental sheet forming. *CIRP Ann.* **2019**, *68*, 317–320. [CrossRef]
158. Fiorentino, A.; Feriti, G.C.; Ceretti, E.; Giardini, C.; Bort, C.M.G.; Bosetti, P. Development of Tool Path Correction Algorithm in Incremental Sheet Forming. *Key Eng. Mater.* **2014**, *622*, 382–389. [CrossRef]
159. Rauch, M.; Hascoet, J.Y.; Hamann, J.C.; Plenel, Y. Tool path programming optimization for incremental sheet forming applications. *Comput. Aided Des.* **2009**, *41*, 877–885. [CrossRef]
160. Behera, A.K.; Verbert, J.; Lauwers, B.; Duflou, J.R. Tool path compensation strategies for single point incremental sheet forming using multivariate adaptive regression splines. *Comput. Des.* **2013**, *45*, 575–590. [CrossRef]
161. Fu, Z.; Mo, J.; Han, F.; Gong, P. Tool path correction algorithm for single-point incremental forming of sheet metal. *Int. J. Adv. Manuf. Technol.* **2013**, *64*, 1239–1248. [CrossRef]
162. Nasulea, D.; Oancea, G. Achieving Accuracy Improvements for Single-Point Incremental Forming Process Using a Circumferential Hammering Tool. *Metals* **2021**, *11*, 482. [CrossRef]
163. Ambrogio, G.; Cozza, V.; Filice, L.; Micari, F. An analytical model for improving precision in single point incremental forming. *J. Mater. Process. Technol.* **2007**, *191*, 92–95. [CrossRef]
164. Micari, F.; Ambrogio, G.; Filice, L. Shape and dimensional accuracy in Single Point Incremental Forming: State of the art and future trends. *J. Mater. Process. Technol.* **2007**, *191*, 390–395. [CrossRef]
165. Isidore, B.B.L.; Hussain, G.; Shamchi, S.P.; Khan, W.A. Prediction and control of pillow defect in single point incremental forming using numerical simulations. *J. Mech. Sci. Technol.* **2016**, *30*, 2151–2161. [CrossRef]
166. Isidore, B.B.L. Controlling Pillow Defect in Single Point Incremental Forming Through Varying Tool Geometry. Master's Thesis, Eastern Mediterranean Universit, Gazimağusa, North Cyprus, June 2014.
167. Zhang, H.; Lu, B.; Chen, J.; Feng, S.; Li, Z.; Long, H. Thickness control in a new flexible hybrid incremental sheet forming process. *Proc. Inst. Mech. Eng. Part B J. Eng. Manuf.* **2017**, *231*, 779–791. [CrossRef]
168. Wei, H.; Hussain, G.; Shi, X.; Isidore, B.B.L.; Alkahtani, M.; Abidi, M.H. Formability of Materials with Small Tools in Incremental Forming. *Chinese J. Mech. Eng.* **2020**, *33*, 55. [CrossRef]
169. Al-Ghamdi, K.; Hussain, G. The pillowing tendency of materials in single-point incremental forming: Experimental and finite element analyses. *Proc. Inst. Mech. Eng. Part B J. Eng. Manuf.* **2015**, *229*, 744–753. [CrossRef]
170. Afzal, M.J. Study on the Single Point Incremental Sheet Forming of AISI 321 Variable Wall Angle Geometry. Available online: https://doi.org/10.21203/rs.3.rs-836822/v1 (accessed on 31 October 2021).
171. Essa, K.; Hartley, P. An assessment of various process strategies for improving precision in single point incremental forming. *Int. J. Mater. Form.* **2011**, *4*, 401–412. [CrossRef]
172. Li, J.; Yang, F.; Zhou, Z. Thickness distribution of multistage incremental forming with different forming stages and angle intervals. *J. Cent. South Univ.* **2015**, *22*, 842–848. [CrossRef]
173. Gonzalez, M.M.; Lutes, N.A.; Fischer, J.D.; Woodside, M.R.; Bristow, D.A.; Landers, R.G. Analysis of geometric accuracy and thickness reduction in multistage incremental sheet forming using digital image correlation. *Procedia Manuf.* **2019**, *34*, 950–960. [CrossRef]
174. Li, J.; Hu, J.; Pan, J.; Geng, P. Thickness distribution and design of a multistage process for sheet metal incremental forming. *Int. J. Adv. Manuf. Technol.* **2012**, *62*, 981–988. [CrossRef]
175. Ambrogio, G.; Gagliardi, F.; Serratore, G.; Ramundo, E.; Filice, L. SPIF of tailored sheets to optimize thickness distribution along the shaped wall. *Procedia Manuf.* **2019**, *29*, 80–87. [CrossRef]
176. Salem, E.; Shin, J.; Nath, M.; Banu, M.; Taub, A.I. Investigation of Thickness Variation in Single Point Incremental Forming. *Procedia Manuf.* **2016**, *5*, 828–837. [CrossRef]
177. Awankar, G.B.; Rathi, M.G.; Brahmagiri, A.S. Experimental Investigation of Thickness Distribution in Incremental Sheet Forming for Aluminium. *J. Mater. Sci. Mech. Eng.* **2015**, *2*, 31–34.
178. Zhu, H.; Cheng, G.; Jung, D. Toolpath Planning and Generation for Multi-Stage Incremental Forming Based on Stretching Angle. *Materials* **2021**, *14*, 4818. [CrossRef]
179. Li, J.; Li, C.; Zhou, T.T. Thickness distribution and mechanical property of sheet metal incremental forming based on numerical simulation. *Trans. Nonferr. Met. Soc. China* **2012**, *22*, s54–s60. [CrossRef]
180. Hrairi, M.; Echrif, S.B.M. Process Simulation and Quality Evaluation in Incremental Sheet Forming. *IIUM Eng. J.* **2011**, *12*, 185–196. [CrossRef]
181. Hussain, G.; Gao, L. A novel method to test the thinning limits of sheet metals in negative incremental forming. *Int. J. Mach. Tools Manuf.* **2007**, *47*, 419–435. [CrossRef]
182. Li, X.; Han, K.; Xu, P.; Wang, H.; Li, D.; Li, Y.; Li, Q. Experimental and theoretical analysis of the thickness distribution in multistage two point incremental sheet forming. *Int. J. Adv. Manuf. Technol.* **2020**, *107*, 191–203. [CrossRef]

183. Avitzur, B.; Yang, C.T. Analysis of Power Spinning of Cones. *J. Eng. Ind.* **1960**, *82*, 231–244. [CrossRef]
184. Young, D.; Jeswiet, J. Wall thickness variations in single-point incremental forming. *Proc. Inst. Mech. Eng. Part B J. Eng. Manuf.* **2004**, *218*, 1453–1459. [CrossRef]
185. Ambrogio, G.; Filice, L.; Gagliardi, F.; Micari, F. Sheet Thinning Prediction in Single Point Incremental Forming. *Adv. Mater. Res.* **2005**, *6*, 479–486. [CrossRef]
186. Bambach, M. A geometrical model of the kinematics of incremental sheet forming for the prediction of membrane strains and sheet thickness. *J. Mater. Process. Technol.* **2010**, *210*, 1562–1573. [CrossRef]
187. Yang, M.; Yao, Z.; Li, Y.; Li, P.; Cui, F.; Bai, L. Study on Thickness Thinning Ratio of the Forming Parts in Single Point Incremental Forming Process. *Adv. Mater. Sci. Eng.* **2018**, *2018*, 1–11. [CrossRef]
188. Cao, T.; Liu, B.; Xu, D.; Zhang, H.; Chen, J.; Long, H.; Cao, J. An efficient method for thickness prediction in multi-pass incremental sheet forming. *Int. J. Adv. Manuf. Technol.* **2015**, *77*, 469–483. [CrossRef]
189. Dohda, K.; Yamamoto, M.; Hu, C.; Dubar, L.; Ehmann, K.F. Galling phenomena in metal forming. *Friction* **2021**, *9*, 665–685. [CrossRef]
190. Pujante, J.; Pelcastre, L.; Vilaseca, M.; Casellas, D.; Prakash, B. Investigations into wear and galling mechanism of aluminium alloy-tool steel tribopair at different temperatures. *Wear* **2013**, *308*, 193–198. [CrossRef]
191. Dabwan, A.; Ragab, A.E.; Saleh, M.A.; Anwar, S.; Ghalab, A.M.; Rehman, A.U. Study of the Effect of Process Parameters on Surface Profile Accuracy in Single-Point Incremental Sheet Forming of AA1050-H14 Aluminum Alloy. *Adv. Mater. Sci. Eng.* **2020**, *2020*, 7265941. [CrossRef]
192. Shamchi, S.P. Microstructures and Mechanical properties of AA-5754 and AA-6061 Aluminum alloys formed by Single Point Incremental Forming Process. Master's Thesis, Eastern Mediterranean University, Gazimağusa, Cyprus, 2014.
193. Viet, M.V.; Thinh, N.T.; Sy, L.V.; Antonov, S. Study on the formability by TPIF technology for aluminium sheet at room temperature. *E3S Web Conf.* **2020**, *207*, 05005. [CrossRef]
194. Azpen, Q.; Beharudin, H.; Sulaiman, S.; Mustapha, F. Effect of process parameters on the surface roughness of aluminum alloy AA 6061-T6 sheets in frictional stir incremental forming. *Adv. Prod. Eng. Manag.* **2018**, *13*, 405–416. [CrossRef]
195. Durante, M.; Formisano, A.; Langella, A.; Minutolo, F.M.C. The influence of tool rotation on an incremental forming process. *J. Mater. Process. Technol.* **2009**, *209*, 4621–4626. [CrossRef]
196. Bhattacharya, A.; Maneesh, K.; Venkata Reddy, N.; Cao, J. Formability and surface finish studies in single point incremental forming. *J. Manuf. Sci. Eng.* **2011**, *133*, 061020. [CrossRef]
197. Hamilton, K.; Jeswiet, J. Single point incremental forming at high feed rates and rotational speeds: Surface and structural consequences. *CIRP Annals* **2010**, *59*, 311–314. [CrossRef]
198. Ambrogio, G.; Filice, L.; Gagliardi, F. Improving industrial suitability of incremental sheet forming process. *Int. J. Adv. Manuf. Technol.* **2012**, *58*, 941–947. [CrossRef]
199. Lasunon, O.U. Surface roughness in incremental sheet metal forming of AA5052. *Adv. Mater. Res.* **2013**, *753–755*, 203–206. [CrossRef]
200. Filice, L.; Fratini, L.; Micari, F. Analysis of material formability in incremental forming. *CIRP Annals* **2002**, *51*, 199–202. [CrossRef]
201. Liu, Z.; Liu, S.; Li, Y.; Meehan, P.A. Modeling and optimization of surface roughness in incremental sheet forming using a multi-objective function. *Mater. Manuf. Process.* **2014**, *29*, 808–818. [CrossRef]
202. Mugendiran, V.; Gnanavelbabu, A.; Ramadoss, R. Parameter optimization for surface roughness and wall thickness on AA5052 aluminium alloy by incremental forming using response surface methodology. *Procedia Eng.* **2014**, *97*, 1991–2000. [CrossRef]
203. Lu, B.; Fang, Y.; Xu, D.K.; Chen, J.; Ou, H.; Moser, N.H.; Cao, J. Mechanism investigation of friction-related effects in single point incremental forming using a developed oblique roller-ball tool. *Int. J. Mach. Tools Manuf.* **2014**, *85*, 14–29. [CrossRef]
204. Powers, B.M.; Ham, M.; Wilkinson, M.G. Small data set analysis in surface metrology: An investigation using a single point incremental forming case study. *Scanning* **2010**, *32*, 199–211. [CrossRef] [PubMed]
205. Singh, S. A review on computer aided manufacturing factors affecting reduction of surface roughness and thickness. *Int. Res. J. Eng. Technol.* **2017**, *4*, 1474–1478.
206. Mulay, A.; Ben, B.S.; Ismail, S.; Kocańda, A.; Jasiński, C. Performance evaluation of high-speed incremental sheet forming technology for AA5754 H22 aluminum and DC04 steel sheets. *Arch. Civ. Mech. Eng.* **2018**, *18*, 1275–1287. [CrossRef]
207. Nama, S.A.; Namer, N.S.M.; Najm, S.M. The effect of using grease on the surface roughness of aluminum 1100 sheet during the Single Point Incremental Forming Process. *Trends Mach. Des.* **2014**, *1*, 53–56.
208. Hagan, E.; Jeswiet, J. Analysis of surface roughness for parts formed by computer numerical controlled incremental forming. *Proc. Inst. MEch. Eng, Part B J. Eng. Manuf.* **2004**, *218*, 1307–1312. [CrossRef]
209. Hussain, G.; Gao, L.; Hayat, N.; Cui, Z.; Pang, Y.; Dar, N. Tool and lubrication for negative incremental forming of a commercially pure titanium sheet. *J. Mater. Process. Technol.* **2008**, *203*, 193–201. [CrossRef]
210. Bambach, M.; Hirt, G.; Junk, S. Modelling and Experimental Evaluation of the Incremental CNC Sheet Metal Forming Process. In Proceedings of the COMPLAS 7: 7th International Conference on Computational Plasticity, Barcelona, Spain, 7–10 April 2003; pp. 1–16.
211. Eyckens, P.; Duflou, J.; Bael, A.; Houtte, P. The significance of friction in the single point incremental forming process. *Int. J. Mater. Form.* **2010**, *3*, 947–950. [CrossRef]
212. Lee, B.H.; Keum, Y.K.; Wagoner, R.H. Modeling of the Friction Caused by Lubrication and Surface Roughness in Sheet Metal Forming. *J. Mater. Process. Technol.* **2002**, *130*, 60–63. [CrossRef]
213. Trzepieciński, T. Tribological Performance of Environmentally Friendly Bio-Degradable Lubricants Based on a Combination of Boric Acid and Bio-Based Oils. *Materials* **2020**, *13*, 3892. [CrossRef]

214. Azevedo, N.G.; Farias, J.S.; Bastos, R.P.; Teixeira, P.; Davim, J.P.; de Sousa, R.J.A. Lubrication aspects during single point incremental forming for steel and aluminum materials. *Int. J. Precis. Eng. Manuf.* **2015**, *16*, 589–595. [CrossRef]

215. Suriyaprakan, P. Single Point Incremental Forming and MultiStage Incremental Forming on Aluminium Alloy 1050. Master's Thesis, University of Porto, Porto, Portugal, February 2013.

216. Gulati, V.; Aryal, A.; Katyal, P.; Goswami, A. Process parameters optimization in single point incremental forming. *J. Inst. Eng. (India) Ser. A* **2016**, *97*, 185–193. [CrossRef]

217. Oraon, M.; Sharma, V. Prediction of surface roughness in single point incremental forming of AA3003-O alloy using artificial neural network. *Int. J. Mater. Eng. Innov.* **2018**, *9*, 1–19. [CrossRef]

218. Patel, J.R.; Samvatsar, K.S.; Prajapati, H.P.; Rangrej, S.S. Optimization of process parameters for reducing surface roughness produced during single point incremental forming process. *Int. J. Recent Technol. Mech. Electrical Eng.* **2015**, *2*, 19–23.

219. Duflou, J.; Tunckol, Y.; Szekeres, A.; Vanherck, P. Experimental study on force measurements for single point incremental forming. *J. Mater. Process. Technol.* **2007**, *189*, 65–72. [CrossRef]

220. Kim, Y.H.; Park, J.J. Effect of process parameters on formability in incremental forming of sheet metal. *J. Mater. Process. Technol.* **2002**, *130–131*, 42–46. [CrossRef]

221. Buffa, G.; Campanella, D.; Fratini, L. On the Improvement of Material Formability in SPIF Operation through Tool Stirring Action. *Int. J. Adv. Manuf. Technol.* **2013**, *66*, 1343–1351. [CrossRef]

222. Xu, D.; Wu, W.; Malhotra, R.; Chen, J.; Lu, B.; Cao, J. Mechanism Investigation for the Influence of Tool Rotation and Laser Surface Texturing (LST) on Formability in Single Point Incremental Forming. *Int. J. Mach. Tools Manuf.* **2013**, *73*, 37–46. [CrossRef]

223. Liu, Z. Friction Stir Incremental Forming of AA7075-O Sheets: Investigation on Process Feasibility. *Procedia Eng.* **2017**, *207*, 783–788. [CrossRef]

224. Duflou, J.R.; Callebaut, B.; Verbert, J.; De Baerdemaeker, H. Improved SPIF Performance through Dynamic Local Heating. *Int. J. Mach. Tools Manuf.* **2008**, *48*, 543–549. [CrossRef]

225. Hino, R.; Yoshida, F.; Nagaishi, N.; Naka, T. Incremental Sheet Forming with Local Heating for Lightweight Hard-to-Form Material. *Int. J. Mod. Phys. B* **2008**, *22*, 6082–6087. [CrossRef]

226. Sy, L.V.; Thanh Nam, N. Hot Incremental Forming of Magnesium and Aluminum Alloy Sheets by Using Direct Heating System. *Proc. Inst. Mech. Eng. Part B J. Eng. Manuf.* **2013**, *227*, 1099–1110.

227. Singh, S.A.; Priyadarshi, S.; Tandon, P. Investigations on the Influence of Heat on AA1050 Sheet during Incremental Forming. *Lett. Mater.* **2019**, *9*, 523–527. [CrossRef]

228. Vahdani, M.; Mirnia, M.J.; Bakhshi-Jooybari, M.; Gorji, H. Electric Hot Incremental Sheet Forming of Ti-6Al-4V Titanium, AA6061 Aluminum, and DC01 Steel Sheets. *Int. J. Adv. Manuf. Technol.* **2019**, *103*, 1199–1209. [CrossRef]

229. Najm, S.M.; Paniti, I.; Trzepieciński, T.; Nama, S.A.; Viharos, Z.J.; Jacso, A. Parametric Effects of Single Point Incremental Forming on Hardness of AA1100 Aluminium Alloy Sheets. *Materials* **2021**, *14*, 7263. [CrossRef]

230. Gupta, P.; Jeswiet, J. Observations on Heat Generated in Single Point Incremental Forming. *Procedia Eng.* **2017**, *183*, 161–167. [CrossRef]

231. Xiao, X.; Kim, C.-I.; Lv, X.-D.; Hwang, T.-S.; Kim, Y.-S. Formability and Forming Force in Incremental Sheet Forming of AA7075-T6 at Different Temperatures. *J. Mech. Sci. Technol.* **2019**, *33*, 3795–3802. [CrossRef]

232. Li, Z.; Lu, S.; Zhang, T.; Zhang, C.; Mao, Z. 1060 Al Electric Hot Incremental Sheet Forming Process: Analysis of Dimensional Accuracy and Temperature. *Trans. Indian. Inst. Met.* **2018**, *71*, 961–970. [CrossRef]

233. Pacheco, P.A.P.; Silveira, M.E. Numerical Simulation of Electric Hot Incremental Sheet Forming of 1050 Aluminum with and without Preheating. *Int. J. Adv. Manuf. Technol.* **2018**, *94*, 3097–3108. [CrossRef]

234. Pacheco, P.A.P.; Silveira, M.E.; Silva, J.A. Heat Distribution in Electric Hot Incremental Sheet Forming. *Int. J. Adv. Manuf. Technol.* **2019**, *102*, 991–998. [CrossRef]

235. Bejan, A.; Kraus, A.D. *Heat Transfer Handbook*; John Wiley & Sons, Inc.: New York, NY, USA, 2003.

236. Darzi, S.; Mirnia, M.J.; Elyasi, M. Single-Point Incremental Forming of AA6061 Aluminum Alloy at Elevated Temperatures. *Int. J. Adv. Manuf. Technol.* **2021**, *116*, 1023–1039. [CrossRef]

237. Zhang, P.; Li, J.; Chen, M. Effect of Different Temperatures on the Metallographic Structure and Tensile Property of 2024-T4 Alloy in Integral Heating Single Point Incremental Forming. *Microsc. Res. Techn.* **2020**, *83*, 920–927. [CrossRef]

238. Rahmani, F.; Seyedkashi, S.M.H.; Hashemi, S.J. Experimental Study on Warm Incremental Tube Forming of AA6063 Aluminum Tubes. *Int. J. Eng.* **2020**, *33*, 1773–1779.

239. Otsu, M.; Katayama, Y.; Muranaka, T. Effect of Difference of Tool Rotation Direction on Forming Limit in Friction Stir Incremental Forming. *Key Eng. Mater.* **2014**, *622–623*, 390–397. [CrossRef]

240. Gupta, P.; Jeswiet, J. Effect of Temperatures during Forming in Single Point Incremental Forming. *Int. J. Adv. Manuf. Technol.* **2018**, *95*, 3693–3706. [CrossRef]

241. Wang, Z.; Cai, S.; Chen, J. Experimental Investigations on Friction Stir Assisted Single Point Incremental Forming of Low-Ductility Aluminum Alloy Sheet for Higher Formability with Reasonable Surface Quality. *J. Mater. Process. Technol.* **2020**, *277*, 116488. [CrossRef]

242. Zhan, X.; Huang, W.; Li, D.; Chen, J. An Optimum Process Window to Preferable Microstructure Distribution and Improved Macroscopic Property for Friction Stir–Assisted Incremental Aluminum Alloy Sheet Forming. *Int. J. Adv. Manuf. Technol.* **2021**, *115*, 1589–1603. [CrossRef]

243. Zhan, X.; Liu, X.; Yang, M.; Li, M.; Li, X.; Chen, J. Dynamic Recrystallization and Solute Precipitation during Friction Stir Assisted Incremental Forming of AA2024 Sheet. *Mater. Charact.* **2021**, *174*, 111046. [CrossRef]

244. Li, M.; Wu, R.; Cai, S.; Chang, Z.; Wang, Z.; Chen, J. Experimental Investigation on Friction-Stir-Assisted Incremental Forming with Synchronous Bonding of Aluminum Alloy and Steel Sheets. *J. Mater. Eng. Perform.* **2020**, *29*, 750–759. [CrossRef]
245. Wu, R.; Li, M.; Liu, X.; Cai, S.; Chen, J. Characterization of Material Flow in Friction Stir-Assisted Incremental Forming with Synchronous Bonding of Dissimilar Sheet Metals. *Int. J. Adv. Manuf. Technol.* **2020**, *109*, 2523–2534. [CrossRef]
246. Wu, R.; Li, M.; Liu, X.; Yang, Z.; Chen, J. Interfacial Quality Prediction Model for Al/Steel Sheets during Friction Stir Assisted Double-Sided Incremental Forming with Synchronous Bonding. Available online: https://www.researchsquare.com/article/rs-531361/v1 (accessed on 1 November 2021).
247. Wu, R.; Liu, X.; Li, M.; Chen, J. Investigations on Deformation Mechanism of Double-Sided Incremental Sheet Forming with Synchronous Thermomechanical Steel-Aluminum Alloy Bonding. *J. Mater. Process. Technol.* **2021**, *294*, 117147. [CrossRef]
248. Mohammadi, A.; Vanhove, H.; Bael, A.; Seefeldt, M.; Duflou, J. The Effect of Laser Radiation on the Residual Stress Levels of Single Point Incrementally Formed (SPIF) Parts. Available online: https://core.ac.uk/download/pdf/34624438.pdf (accessed on 1 November 2021).
249. Lehtinen, P.; Väisänen, T.; Salmi, M. The Effect of Local Heating by Laser Irradiation for Aluminum, Deep Drawing Steel and Copper Sheets in Incremental Sheet Forming. *Phys. Procedia* **2015**, *78*, 312–319. [CrossRef]
250. Mohammadi, A.; Vanhove, H.; van Bael, A.; Weise, D.; Duflou, J.R. Formability Enhancement in Incremental Forming for an Automotive Aluminium Alloy Using Laser Assisted Incremental Forming. *Key Eng. Mater.* **2015**, *639*, 195–202. [CrossRef]
251. Mohammadi, A.; Qin, L.; Vanhove, H.; Seefeldt, M.; Van Bael, A.; Duflou, J.R. Single Point Incremental Forming of an Aged AL-Cu-Mg Alloy: Influence of Pre-Heat Treatment and Warm Forming. *J. Mater. Eng. Perform.* **2016**, *25*, 2478–2488. [CrossRef]